Anonymous Referee #1

Received and published: 6 August 2019

Authors' response: We are grateful to Anonymous Referee #1 for the time and useful comments. We have made point-to-point responses to each question in blue text below. Please note that line numbers correspond to the revised manuscript.

(I apologize in advance for not figuring out the LaTeX commands for "del" and "per mil" symbols for my comments.)

This paper discusses the results of measurements of the isotopic composition of NOx, HONO, and particle nitrate emission from laboratory biomass burns done as part of the FIREX campaign. This represents the first measurements of the isotopic composition of HONO from biomass burning, a critical component of the smoke radical budget in the ambient atmosphere. They find that the isotopic composition of the HONO and NOx is well corelated, suggesting they are formed via similar pathways.

The paper is very well-written and while I am not competent to evaluate the analytical chemistry methods used, they are described thoroughly in the paper and it is clear the authors put a lot of thought into their experimental setup. The results are clearly explained and the conclusions follow from the evidence presented in the paper. Overall, this is a very good manuscript and should be published after minor revisions to address my minor concerns listed below.

L20: Missing and "and" before "proton-transfer-reaction"

Authors' response:

Corrected. Thank you!

L31: "connected via formation pathways" is a very vague phrase. Can you be more specific about how they are linked here?

Authors' response:

Modified. Please see L23-24, "NOx and HONO are connected via formation pathways" is changed to "HONO is directly formed via subsequent chain reactions of NO_x emitted from biomass combustion"

L33: It seems odd to mention the importance of your particle nitrate measurements here, since you didn't think they were important enough to mention the quantitative results in the previous paragraph. Can you please add those results to the abstract?

Authors' response:

We added the isotopic composition results for particulate nitrate in the abstract. Please see L24-26.

L38-39: Why are the del18O measurements for each species expected to track with the influence of ozone, photochemistry and nighttime chemistry? That isn't obvious to me.

Authors' response:

O_3 has uniquely high $\delta^{18}O$ value (~110‰) that can be distinguished from other oxidants including O_2, OH, and HO_2 (< ~20‰), therefore formation pathways of secondary products such as NO_2, HONO, HNO_3 and particulate nitrate may be distinguished with $\delta^{18}O$ value of these products. For example, NO_2 formed from $NO+O_3$ will exhibit much higher $\delta^{18}O$-NO_2 than that formed from $NO+HO_2/RO_2$. Nighttime HNO_3 is mainly formed from $NO+O_3 \rightarrow NO_2$, $NO_2+O_3 \rightarrow NO_3$, $NO_2+ NO_3 \rightarrow N_2O_5$, and $N_2O_5+H_2O \rightarrow 2HNO_3$. Therefore, HNO_3 formed during the night has higher $\delta^{18}O$ than during the day.

L49: While everyone knows what cooking and heating are, "prescribed" is an uncommon term and should be defined. I'd also refer to "prescribed burning" to match the "ing"s in the other terms.

Authors' response:

Corrected and "prescribed burning" is defined in the text (L49). Thanks!

L93-96: This sentence is hard to understand, with many "and"s stringing things together. Can you please rephrase, maybe splitting into two sentences to make the meaning clearer?

Authors' response:

This sentence has been split in to two sentences as shown in L94-97. Thanks!

L152-154: I have no idea how these acronyms were made – how did "subalpine fir" become "ABLA"? Not critical as you define them, but it was a strange choice that left me constantly flipping back to understand what was burning.

Authors' response:

This is a good point. The acronyms are defined based on Latin names of the vegetation species, as you can see in this example (https://plants.usda.gov/core/profile?symbol=PICO)

For readers' convenience, all the acronyms have been replaced by corresponding names.

L236-237: Please describe how you corrected the NOx for HONO interference, as you say on L235 that HONO is partially, not completely, converted on the catalyst.

Authors' response:

Thank you for asking this question. "Partially" was used in the original manuscript to discuss the NOy interference species in a qualitative and conservative way. The catalytic

efficiency of NOy species other than NO2 to NO were not measured for this particular Thermo NOx analyzer, however a number of previous works found the HONO (e.g. Febo et al 1995) conversion efficiency is high and deemed the conversion efficiency 100%. We correct the NOx concentration by subtracting mean HONO concentration during each period from NOx concentration, and this provided an approximate lower limit of NOx concentration with upper limit of HONO concentration.

L341-342: I'm assuming the bacteria preserves the isotope ratios and/or you can correct for the effect of the bacteria, but that isn't obvious to me, so you might want to clarify that here.

Authors' response:

The bacteria method can preserve the isotopic signature of NO_3^- and/or NO_2^- so I replace "quantitative" with "complete" in the original sentence (L321). Thanks for the suggestion.

L388-394: Your explanation for the low HONO values in Fire #12 being linked to smoldering combustion and lower MCE (0.87) isn't very convincing, as Fire #15, which you note on L385-387 had the highest HONO, had an MCE of 0.89, as did Fire #17. My guess is you don't have enough information to really explain why Fire 12 was anomalously low in HONO, but in any case, you need to revise this section to include the caveat about the MCE of Fire #15.

Authors' response:

This is a really great question and thank you!

We agree with the reviewer's comment on MCE and we note for fire #12 the strong smoldering resulted in clogging of the inlet filter of the MC/IC that significantly impact the measured HONO concentration by MC/IC. Accordingly, we added the following (L369-372 and L378-382 respctively):

"We note that fire no. 12 has the smallest MCE value of 0.868 (FIREX, 2016), and an abnormal flow rate (less than half of the typical flow rate during all other measurements) due to the inlet filter clogging from extraordinarily large particulate loadings."

"Although fires no. 15 and no. 17 have relatively low MCE (~0.89), the pulse of HONO in first 5-10 minutes suggest an active flaming phase followed by longer smoldering phase. This indicates both fires had combustion conditions that consisted of a mixture of flaming and smoldering, and thus significant HONO was still produced."

L435 and elsewhere: Since you have both positive and negative values, I'd use the word "to" instead of the n-dash symbol to connect the ranges. i.e. "-4.3 per mil to +7.0 per mil" instead of "-4.3 per mil - +7.0 per mil."

Data availability: Consider using the CERN Zenodo archive (zenodo.org) or similar free service to store the data in a public repository with a unique DOI.

Figure 1 caption: Mention that the HONO and HNO3 in these plots was measured using the MC/IC method from the text

Table S1 caption: Please make a more descriptive caption.

Table S2 caption: Please explain why some data are missing (below detection limit? Instrument error?)

Figure S1 caption: Please clarify what the p values are for, e.g., the slope of a linear correlation?

Figure S2 caption: The caption is hard to understand. Try "Linear regression between (a) del15N-HONO and del15N-biomass (equation) and (b). . ." instead.

Isotopic characterization of nitrogen oxides (NO$_x$), nitrous acid (HONO), and nitrate (NO$_3^-$(p)) from laboratory biomass burning during FIREX

Jiajue Chai[1], David J. Miller[1,a], Eric Scheuer[2], Jack Dibb[2], Vanessa Selimovic[3], Robert Yokelson[3], Kyle J. Zarzana[4,5,b], Steven S. Brown[4,6], Abigail R. Koss[4,5,6,c], Carsten Warneke[5,6], Meredith Hastings[1]

1. Department of Earth, Environmental and Planetary Sciences, and Institute at Brown for Environment and Society, Brown University, Providence, RI, USA
2. Institute for the Study of Earth, Ocean and Space, University of New Hampshire, Durham, NH, USA
3. Department of Chemistry, University of Montana, Missoula, USA
4. Chemical Sciences Division, NOAA Earth System Research Laboratory, Boulder, CO, USA
5. Cooperative Institute for Research in Environmental Sciences, University of Colorado, Boulder, CO, USA
6. Department of Chemistry, University of Colorado, Boulder, CO, USA
a. Now at: Environmental Defense Fund, Boston, MA, USA
b. Now at: Department of Chemistry, University of Colorado, Boulder, CO, USA
c. Department of Civil and Environmental Engineering, Massachusetts Institute of Technology, Cambridge, MA, USA

Correspondence: Jiajue Chai (jiajue_chai@brown.edu)

Abstract

New techniques have recently been developed and applied to capture reactive nitrogen species including nitrogen oxides (NO_x = NO + NO_2), nitrous acid (HONO), nitric acid (HNO_3) and particulate nitrate (NO_3^-(p)), for accurate measurement of their isotopic composition. Here, we report – for the first time – the isotopic composition of HONO from biomass burning (BB) emissions collected during the Fire Influence on Regional to Global Environments Experiment (FIREX, later evolved into FIREX-AQ) laboratory experiments at the Missoula Fire Science Laboratory in the fall of 2016. Using our newly developed annular denuder system (ADS), which was verified to completely capture HONO associated with BB via comparison with 4 other high time resolution concentration measurement techniques, including mist chamber/ion chromatography (MC/IC), open-path Fourier transform infrared spectroscopy (OP-FTIR), cavity enhanced spectroscopy (CES), and proton-transfer-reaction time-of-flight mass spectrometer (PTR-ToF).

In 20 "stack" fires (direct emission within ~5 seconds of production by the fire) that burned various biomass materials from the Western U.S., δ^{15}N-NO_x ranges from -4.3 ‰ to +7.0 ‰, falling near the middle of the range reported in previous work. The first measurements of δ^{15}N-HONO and δ^{18}O-HONO in biomass burning smoke reveal a range of -5.3‰ to +5.8‰ and +5.2‰ to +15.2‰, respectively. Both HONO and NO_x are sourced from N in the biomass fuel and δ^{15}N-HONO and δ^{15}N-NO_x are strongly correlated (R^2 = 0.89, p<0.001), suggesting HONO is directly formed via subsequent chain reactions of NO_x emitted from biomass combustion. Only 5 of 20 NO_3^-(p) samples had a sufficient amount for isotopic analysis, and showed δ^{15}N and δ^{18}O of NO_3^-(p) range from -10.6‰ to -7.4 ‰ and +11.5‰ to +14.8‰ respectively.

Our δ^{15}N of NO_x, HONO and NO_3^-(p) ranges can serve as important biomass burning source signatures, useful for constraining emissions of these species in environmental applications. The δ^{18}O of HONO and NO_3^- obtained here verify our method is capable of determining the oxygen isotopic composition in BB plumes. The δ^{18}O for both of these species reflect laboratory conditions (i.e. a lack of photochemistry), and would be expected to track with the influence of different oxidation pathways in real environments. The methods used in this study will be further applied in future field studies to quantitatively track reactive nitrogen cycling in fresh and aged Western US wildfire plumes.

1 Introduction

Biomass burning (BB), which occurs in both anthropogenic processes (e.g. cooking, heating, and prescribed burning that is human controlled burning for management purpose) and natural wildfire (lightning ignited vegetation burning), is a significant source of atmospheric reactive nitrogen species, including nitrogen oxides ($NO_x = NO + NO_2$), nitrous acid (HONO), nitric acid (HNO_3), particulate nitrate (NO_3^-(p)), organic nitrates, peroxyacyl nitrate (PAN) and ammonia (NH_3) that have major impacts on air quality and climate from regional to global scales (Crutzen and Andreae, 1990). Globally, biomass burning emits ~6 Tg of nitrogen oxides ($NO_x = NO + NO_2$) per year, contributing at least 14% to total NO_x emissions (Jaeglé et al., 2005), with large interannual and seasonal variation due to fire frequency and intensity (Jaffe and Briggs, 2012). Primarily emitted NO_x plays an important role in the photo-oxidation of volatile and semi volatile organic compounds, which are present in high concentrations in BB plumes, and strongly influences production of tropospheric ozone (O_3) and secondary aerosols (Alvarado et al., 2015). In BB plumes, NO_x can be converted to PAN, which can be transported long distances (100s to 1000s of km) in lofted plumes before rereleasing NO_x. Therefore, BB emitted NO_x could widely influence air quality downwind for days to weeks (Val Martín et al., 2006; Ye et al., 2016). In addition, NO_x is also the major photochemical precursor of HNO_3 and NO_3^-(p), which can be transported downwind, mix with anthropogenic emissions, and impact air quality and ecosystem health (Hastings et al., 2013).

HONO has been observed in BB plumes in both laboratory and field experiments, with HONO mixing ratios in the range of ~5-33% of observed NO_x (Akagi et al., 2012, 2013; Burling et al., 2010, 2011; Keene et al., 2006; Liu et al., 2016; Roberts et al., 2010; Selimovic et al., 2018; Yokelson et al., 2007, 2009). Photolysis of HONO is a major OH precursor in the daytime; therefore HONO plays an important role in photochemical aging of BB plumes and atmospheric oxidation capacity at regional scales (Alvarado and Prinn, 2009; Liu et al., 2016; Tkacik et al., 2017; Trentmann et al., 2005). HONO has been proposed as a significant OH source in BB plumes and the inclusion of HONO in photochemical models could explain much of the uncertainty in the modeled O_3 (Alvarado et al., 2009; Alvarado and Prinn, 2009; Cook et al., 2007; Travis et al., 2016; Trentmann et al., 2005).

Direct BB emission factor measurements of HONO and NO_x exhibit significant uncertainties due to limited observations and large spatial and temporal variability of burning conditions, making it challenging to build an accurate inventory of BB emissions relative to other major sources (Lapina et al., 2008). Emission factors vary and mainly depend on 1) fuel nitrogen content (0.2 – 4% by mass), which is a function of vegetation type, and 2) modified combustion efficiency (MCE = $\Delta[CO_2]/(\Delta[CO] + \Delta[CO_2])$) that is determined by combustion conditions including fuel moisture, fuel load, temperature, relative humidity, wind speed, and other meteorological parameters (Burling et al., 2010; Jaffe and Briggs, 2012; Yokelson et al., 1996). Additionally, the temporal evolution of HONO in BB plumes varies greatly in different fires and relative contributions from direct emission versus NO_2 conversion to HONO remains unclear. For instance, significant concentrations of HONO and correlation between HONO and NO_2 have been observed in aged plumes, indicating the importance of heterogeneous conversion of NO_2–

3

92 to–HONO on BB aerosols (Nie et al., 2015). By contrast, no evidence was found for
93 secondary HONO formation in a BB plume during the Southeast Nexus Experiment
94 (Neuman et al., 2016). It is important to constrain HONO directly emitted from BB
95 compared to HONO formed during plume aging. This would reduce uncertainties
96 associated with the total HONO budget and increase our understanding of HONO
97 impacts on O_3 and secondary aerosol formation downwind of BB regions.
98
99 In an effort to better understand reactive nitrogen emissions and chemistry, especially for
100 HONO, new techniques have been developed to analyze the isotopic composition of
101 various species. Stable isotopes provide a unique approach of characterizing and tracking
102 various sources and chemistry for a species of interest (Hastings et al., 2013). Fibiger et
103 al. (2014) developed a method to quantitatively collect NO_x in solution as NO_3^- for
104 isotopic analysis, which has been verified to avoid any isotopic fractionation during
105 collection in both lab and field studies. This allows for high-resolution measurement of
106 $\delta^{15}N$-NO_x in minutes to hours depending on ambient NO_x concentrations ($\delta^{15}N$ =
107 $[(^{15}N/^{14}N)_{sample}/(^{15}N/^{14}N)_{air-N2} - 1] \times 1000‰$, and $\delta^{18}O = [(^{18}O/^{16}O)_{sample}/(^{18}O/^{16}O)_{VSMOW} -$
108 $1] \times 1000‰$ where VSMOW is Vienna Standard Mean Ocean Water). $\delta^{15}N$ has also been
109 used to track gaseous NO_x from a variety of major sources including emissions from
110 biomass burning (Fibiger and Hastings, 2016), vehicles (Miller et al., 2017), and
111 agricultural soils (Miller et al., 2018). Using this method, Fibiger and Hastings (2016)
112 systematically investigated BB $\delta^{15}N$-NO_x from different types of biomass from around
113 the world in a controlled environment during the fourth Fire Lab at Missoula Experiment
114 (FLAME-4). NO_x emissions collected both immediately from the BB source and 1-2
115 hours after the burn in a closed environment ranged from -7 to +12‰, and primarily
116 depended on the $\delta^{15}N$ of the biomass itself. BB emitted HONO isotopic composition has
117 never been measured before. Our recently developed method for HONO isotopic
118 composition analysis (Chai and Hastings, 2018) enables us to not only characterize $\delta^{15}N$
119 and $\delta^{18}O$ of HONO, but also explore the connection between $\delta^{15}N$-NO_x and $\delta^{15}N$-HONO.
120
121 The Fire Influence on Regional to Global Environments and Air Quality (FIREX-AQ)
122 investigates the influence of fires in the western U.S. on climate and air quality, via an
123 intensive, multi-platform, campaign. The first phase of FIREX-AQ took place at the US
124 Forest Service Fire Sciences Laboratory (FSL) in Missoula, Montana, in the fall of 2016,
125 where we measured $\delta^{15}N$-NO_x, $\delta^{15}N$-HONO, $\delta^{18}O$-HONO, $\delta^{15}N$-NO_3^-(p), $\delta^{18}O$-NO_3^-(p)
126 and $\delta^{15}N$-biomass in 20 "stack burns" of a variety of fuels representative of northwestern
127 North America. Here we report on the results and explore relationships between the
128 isotopic composition of these reactive nitrogen species, as well as the corresponding
129 mixing ratios for HONO that were concurrently measured by a variety of techniques.
130 This work offers characterization and quantification of BB source signatures of these
131 species, which can be applied in the interpretation of observations in future field studies.
132
133
134
135
136
137

2. Experimental details
2.1 FIREX Fire Science Laboratory design

The room for controlled BB experiments is 12.5 × 12.5 m × 22 m, with a continuously weighed fuel bed at the center of the room. The combustion exhaust was vented at a constant flow rate (~3.3 m s^{-1}) through a 3.6 m diameter inverted funnel followed by a 1.6 m diameter stack, and collected at a platform 17 m above the fuel bed via sampling ports that surround the stack, resulting in a transport time of ~5 s. Further details have been described in the literature (Stockwell et al., 2014). All of our instruments for sampling and online measurements were placed on the platform, which can accommodate up to 1820 kg of equipment and operators. Measurements were focused on the "stack burns", for which fires lasted a few minutes up to 40 minutes.

For this study, we investigated 20 stack fires of vegetation types abundant in the western US, representing coniferous ecosystems, including ponderosa pine (PIPO), lodgepole pine (PICO), Engelmann spruce (PIEN), Douglas-fir (PSME) and subalpine fir (ABLA), with replicate burns for most of these types (Table 1). Some of the fires proceeded by burning of an individual fuel component such as litter, canopy, duff and rotten logs. Other fires simulated actual biomass in the coniferous ecosystem by mixing various fuel components in realistically recreated ecosystem matrices using the first order fire effects model (FOFEM) (Reinhardt et al., 1997).

2.2 Instrumentation

2.2.1 Collection of HONO, NO$_x$ and nitrate for isotopic analysis
HONO was completely collected for isotopic analysis using an annular denuder system (ADS) (Chai and Hastings, 2018). The ADS system deployed in this laboratory experiment consisted of a Teflon particulate filter, a Nylasorb filter to remove HNO$_3$, followed by two annular denuders, each coated with a solution of 10 mL of Na$_2$CO$_3$ (1% w/v) + glycerol (1% v/v) + methanol−H$_2$O solution (1:1 volume ratio) following a standard EPA method. Methanol and glycerol are certified ACS plus with a purity of ≥99.8% and ≥99.5%, respectively. After coating, the denuders are dried using zero air and capped immediately. Within 6 hours after each collection, the coating was extracted in 10 mL of ultrapure water (18.2 MΩ) in two sequential 5 mL extractions. The extracted solution with a pH of ~10 was transported to Brown University for concentration and isotopic analysis 3-14 days after the sampling. The timescales for sample extraction and isotopic analysis preserve both the solution concentration and isotopic composition of HONO in the form of nitrite (Chai and Hastings, 2018). The two-denuder set up allows us to minimize the interference for both concentration and isotopic analysis from other N-containing species that could be trapped and form nitrite in residual amounts on the denuders, especially NO$_2$. Our method development study showed NO$_2$ tends to absorb in the same amount (difference <4%) on the walls of each denuder in a train setup, which is consistent with other studies (Perrino et al., 1990; Zhou et al., 2018). On the basis of this validation, the second denuder extract is used to correct the first denuder extract for both concentration and isotopic composition (Chai and Hastings, 2018). Note HONO levels

184 were above the minimum detection limit (0.07 μM) and the breakthrough amount of
185 HONO threshold is far from being reached given the concentrations (Table 1), flow rate
186 (~ 4 L/min) and collection times (5 - 40 min). The necessary minimum amount of nitrite
187 collected for isotopic analysis is 10 - 20 nmol.
188
189 To avoid scrubbing of HONO, a flow meter (Omega) and the NO_x collection system for
190 analysis of $\delta^{15}N$-NO_x are placed following the ADS (Fibiger et al., 2014; Fibiger and
191 Hastings, 2016; Wojtal et al., 2016). In brief, NO_x is collected in a solution containing
192 0.25 M $KMnO_4$ and 0.5 M NaOH which oxidizes NO and NO_2 to NO_3^- by pumping
193 sampled air through a gas washing bottle with a 65 Watts diaphragm vacuum pump. The
194 flow rate (~4L/min with ±1% uncertainty) is controlled with a critical orifice inserted
195 between the pump and gas stream outlet, and is monitored and recorded with a flow
196 meter placed prior to the NO_x collector. The NO_x trapping solution blanks are also
197 collected every day to quantify background NO_3^- for concentration and isotopic blank
198 corrections. The Omega flow meter was calibrated with another flow meter (Dry Cal Pro)
199 by varying flow rates. Within a day after collection, we stabilized the samples in the wet
200 chemistry lab in the Fire Science Lab by adding 30% w/w H_2O_2 that reduces MnO_4^- to
201 MnO_2 precipitate before being shipped back to Brown University for further processing.
202 This effectively excludes the possible interferences from NH_3 that could be oxidized to
203 NO_3^- by MnO_4^- after a week (Miller et al. (2017) and references therein). The samples
204 were neutralized with 12.1 N HCl in the Brown lab, before concentration measurement
205 and isotopic analyses. NO_3^- on the upstream Millipore filters and HNO_3 from the
206 Nylasorb filters, if there was any, were extracted by sonicating the filters in ~30 mL
207 ultrapure H_2O (18.2 MΩ) for 30 minutes. Samples with $[NO_3^-] > 1$ μM were analyzed for
208 isotopic composition (concentration techniques detailed below).
209
210 All treated samples from both HONO collection and NO_x collection and their
211 corresponding blanks were analyzed offline for concentrations of NO_2^- and NO_3^- with a
212 WestCo SmartChem 200 Discrete Analyzer colorimetric system. The reproducibility of
213 the concentration measurement was ±0.3 μmol L^{-1} (1σ) for NO_2^- and ±0.4 μmol L^{-1} for
214 NO_3^- when a sample was repeatedly measured (n = 30). A detection limit of 0.07 μmol
215 L^{-1} for NO_2^- and 0.1 μmol L^{-1} for NO_3^- was determined, and no detectable nitrite or
216 nitrate was found in the blank denuder coating solution, whereas blank NO_3^-
217 concentrations of ~5 μM are typical for the NO_x collection method (Fibiger et al., 2014;
218 Wojtal et al., 2016). Note that NO_3^- concentration was measured on the ADS solutions to
219 verify whether and to what extent NO_2^- was oxidized to NO_3^- on denuder walls because
220 the denitrifier method converts both NO_3^- and NO_2^- to N_2O for isotopic analysis (see
221 below). In addition, samples collected with a mist chamber/ion chromatography system
222 (described in Sect. 2.2.2) were also tested for their concentrations and only those with
223 sufficient nitrite quantity were further analyzed for isotopic composition.
224
225 **2.2.2 NO_x and HONO online concentration measurement**
226 NO and NO_x concentrations were measured with a Thermo Scientific Model 42i
227 chemiluminescence NO/NO_x analyzer, which is described in supplemental information.
228 The NO_x measurement verified the concentration of the NO_x collected for isotopic
229 analysis, shown in Table S3 and Figure S1.

230 HONO and HNO$_3$ concentrations were measured using the University of New
231 Hampshire's dual mist chamber/ion chromatograph system (Scheuer et al., 2003) with the
232 sampling inlet placed right next to that of the ADS. The dual channel IC system is custom
233 built using primarily Dionex analytical components. Briefly, automated syringe pumps
234 are used to move samples and standard solutions in a closed system, which minimizes
235 potential contamination. A concentrator column and 5 ml injections were used to improve
236 sensitivity. Eluents are purged and maintained under a pressurized helium atmosphere.
237 Background signal is minimized using electronic suppression (Dionex-ASRS). The
238 chromatography columns and detectors are maintained at 40 °C to minimize baseline
239 drifting. A tri-fluoro-acetate tracer spiked into the ultra-clean sampling water is used as
240 an internal tracer of sample solution volume, which can decrease due to evaporation in
241 the exhaust flow by 10-20% depending on the ambient conditions and length of the
242 sample integration interval. The spike was analyzed to correct the final mist chamber
243 sampled solution volume with an uncertainty of ±3%. This system has been deployed to
244 various field studies for HONO measurement (Dibb et al., 2002; Stutz et al., 2010) and
245 showed reasonable intercomparison with other HONO measurement techniques (within
246 16% uncertainty) during the 2009 SHARP campaign in Houston (Pinto et al., 2014). The
247 detection limits for HNO$_3$ and HONO are 10 ppt for 5-minute sample integrations.
248 During the experiments, two mist chambers were operated to collect gas samples in
249 parallel, each with an integration interval of 5 minutes. One channel of the IC was
250 utilized for concentration measurement; in the other, the mist chamber's solution was
251 transferred into a sample bottle using the syringe pump, and the collected solution was
252 brought to Brown University for isotopic analysis of HNO$_3$ if sufficient amount (10-20
253 nmol) was collected for each sample.
254
255 In addition to MC/IC, the HONO mixing ratios were also measured using high time-
256 resolution (~1 second) measurement techniques including open-path Fourier transform
257 infrared spectroscopy (OP-FTIR) (Selimovic et al., 2018), cavity enhanced spectrometer
258 (CES) (Min et al., 2016; Zarzana et al., 2018), and proton-transfer-reaction time-of-flight
259 mass spectrometer (PTR-ToF). Inlet ports of CES and PTR-ToF were placed 5' apart
260 from, but at the same height on the platform as those for ADS and MC/IC, while the OP-
261 FTIR had an open path cell at the stack. The smoke has been shown to be well-mixed at
262 the sampling platform (Christian et al., 2004) and the mean HONO mixing ratios across
263 each fire obtained from the four techniques were compared with that retrieved from ADS
264 collection. This offers comprehensive verification of complete capture of HONO by ADS
265 that is extremely important for conserving the isotopic composition of HONO.

266 The details of OP-FTIR are described in previous works (Selimovic et al., 2018;
267 Stockwell et al., 2014). The setup included a Bruker MATRIX-M IR cube spectrometer
268 with a mercury cadmium telluride (MCT) liquid-nitrogen-cooled detector interfaced with
269 a 1.6 m base open-path White cell. The white cell was positioned on the platform and its
270 open path spanned the width of the stack. This facilitates direct measurement across the
271 rising emissions. The optical path length was set to 58 m. The IR spectra resolution was
272 0.67 cm^{-1} from 600–4000 cm^{-1}. Pressure and temperature were continuously recorded
273 with a pressure transducer and two temperature sensors respectively, which were placed
274 adjacent to the White cell optical path. They were used for spectral analysis. Time
275 resolution for stack burns was approximately 1.37 s. The OP-FTIR measures CO$_2$, CO,

276 CH$_4$, a series of volatile organic compounds and various reactive nitrogen species
277 (Selimovic et al., 2018). Mixing ratios of HONO were retrieved via multicomponent
278 fitting to a section of the mid-IR transmission spectra with a synthetic calibration
279 nonlinear least-squares method (Griffith, 1996; Yokelson et al., 2007), and both the
280 HITRAN spectral database and reference spectra recorded at the Pacific Northwest
281 National Laboratory (Rothman et al., 2009; Sharpe et al., 2004; Johnson et al., 2010,
282 2013) were used for the fitting. The uncertainty is ~10% for the HONO mixing ratio
283 measurement and the detection limit is no more than a few ppb as reported in previous
284 studies (Stockwell et al., 2014; Veres et al., 2010).

285 HONO measurements by cavity enhanced spectroscopy used the airborne cavity
286 enhanced spectrometer, ACES, recently described by Min *et al.* (2016). This instrument
287 consists of two channels, one measuring over the spectral range from 438-468 nm where
288 glyoxal (CHOCHO) and NO$_2$ have structured absorption bands, and one measuring over
289 from 361-389 nm, where HONO has structured absorption. In the HONO channel, light
290 from an LED centered at 368 nm and with an output power of 450 mW and collimated
291 with an off-axis parabolic collector illuminates the input mirror of a 48 cm optical cavity
292 formed from mirrors with a maximum reflectivity R = 99.98% at 375 nm. The effective
293 path length within the optical cavity is > 3 km over the region of greatest reflectivity. The
294 mirror reflectivity (effective path length) was calibrated from the difference in Rayleigh
295 scattering between Helium and zero air to provide an absolute calibration of the
296 instrument response. A fiber optic bundle collects light exiting the optical cavity and
297 transmits it to a grating spectrometer with a CCD detector, where it is spectrally
298 dispersed at a resolution of 0.8 nm. The resulting spectra are fit using DOASIS software
299 (Kraus, 2006) to determine trace gas concentrations, including NO$_2$, HONO and O$_4$.
300 Mixing ratios of NO$_2$ and HONO are reported at 1 s resolution, although the NO$_2$
301 precision is higher in the 455 nm channel. The 1 Hz HONO precision is 800 pptv (2σ).
302 (The precision of the HONO instrument in ACES is somewhat degraded by the
303 optimization of 455 nm channel for glyoxal detection, which reduces the photon count
304 rate on the 368 nm channel.) The accuracy of the HONO measurement is 9%. Air was
305 sampled directly from stack at a height of 15 m above the fuel bed through a 1 m length
306 of ¼" O.D. Teflon (FEP) tubing as described in Zarzana *et al.* (2018). The residence time
307 in the inlet and sample cells was < 1 s. Comparison between the ACES HONO and an
308 open path FTIR agreed to within 13% on average, and ACES HONO was well correlated
309 with 1Hz measurements from a PTR-ToF (r^2 = 0.95) (Koss et al., 2018).

310 The PTR-ToF instrument used in the FIREX Fire Lab experiment is described in detail in
311 previous studies (Koss et al., 2018; Yuan et al., 2016). The PTR-ToF instrument is a
312 chemical ionization mass spectrometer typically using H$_3$O$^+$ reagent ions and a wide
313 range of trace gases can be detected in the range of tens to hundreds of parts per trillion
314 (pptv) for a 1 s measurement time. At the Fire Lab, PTR-ToF detected several inorganic
315 species including HONO with an uncertainty of 15%. HONO is detected at a lower
316 sensitivity than most trace gases in PTR-ToF, but mixing ratios for all fires were well
317 above the detection limit.

318
319 **2.2.3 Isotopic composition measurements**

320　The denitrifier method was used to perform nitrogen and oxygen isotope analyses
321　($^{15}N/^{14}N$, $^{18}O/^{16}O$) of NO_3^- and/or NO_2^-, by complete conversion to N_2O by denitrifying
322　bacteria *P. aureofaciens* (Casciotti et al., 2002; Sigman et al., 2001). The isotopic
323　composition of N_2O is then determined by a Thermo Finnegan Delta V Plus isotope ratio
324　mass spectrometer at *m/z* 44, 45 and 46 for $^{14}N^{14}N^{16}O$, $^{14}N^{15}N^{16}O$ and $^{14}N^{14}N^{18}O$,
325　respectively. Sample analyses were corrected against replicate measurements of the NO_3^-
326　isotopic reference materials USGS34, USGS35, and IAEA-NO-3 (Böhlke et al., 2003).
327　Additional correction was performed for $\delta^{18}O$-HONO following previous studies
328　(Casciotti et al., 2002, 2007; Chai and Hastings, 2018). Precisions for $\delta^{15}N$-HONO, $\delta^{18}O$-
329　HONO and $\delta^{15}N$-NO_x isotopic analysis across each of the entire methods are ±0.6‰,
330　±0.5‰ and ±1.3‰, respectively (Chai and Hastings, 2018; Fibiger et al., 2014). $\delta^{18}O$-
331　N_2O from the NO_x collection samples was measured but is not reported as $\delta^{18}O$-NO_x
332　because it is greatly impacted by MnO_4^- oxidation and does not represent the $\delta^{18}O$-NO_x in
333　the sample air. The total $\delta^{15}N$ of the starting biomass ($\delta^{15}N$-biomass) was measured at the
334　Marine Biological Laboratory Ecosystems Center Stable Isotope Facility. The materials
335　measured for $\delta^{15}N$-biomass (Table S1) cover most but not all the biomass types burned in
336　the experiments depending on availability of the leftover materials. Analyses were
337　conducted using a Europa ANCA-SL elemental analyzer−gas chromatograph preparation
338　system interfaced with a Europa 20−20 continuous-flow gas source stable isotope ratio
339　mass spectrometer. Analytical precision was ±0.1‰, based on replicate analyses of
340　international reference materials.

341　Collection time spanned the whole fire burning (5 min to 40 min) in order to maximize
342　the signal. We chose to report the samples whose concentrations are at least 30% above
343　the 5 μM NO_3^- present in the blank $KMnO_4$ solution upon purchase (Fibiger et al., 2014),
344　such that the propagated error through the blank correction does not exceed the analytical
345　precision of ±1.5‰ for $\delta^{15}N$-NO_x. We found identical concentration and isotopic
346　signatures for both Fire Lab and Brown University Lab blanks, which ensures that no
347　additional NO_3^- contamination was introduced into the $KMnO_4$ solutions in the gas-
348　washing bottle. In addition, fires with high particulate loading that resulted in >50%
349　reduction in flow rate are not considered for isotopic analysis because the low flow rate
350　could induce incomplete collection with potential isotopic fractionation that might not
351　represent BB emissions.
352
353　**3. Results and discussion**
354
355　**3.1 Temporal evolution of HONO and HNO_3 from direct BB emissions**
356
357　The time series of HONO and HNO_3 concentrations measured by MC/IC at 5-minute
358　resolution for majority of the stack burns are shown in Fig. 1, and original data can be
359　found in the NOAA data archive (FIREX, 2016). HNO_3 concentrations were nearly two
360　orders of magnitude lower than typical HONO concentrations. The constant low
361　concentration of HNO_3 from fresh emissions across all fires is consistent with the
362　findings in Keene et al. (2006), confirming HNO_3 is not a primary reactive nitrogen
363　species in fresh smoke. Rather, it is largely produced secondarily in aged smoke and
364　nighttime chemistry. Both HONO and HNO_3 mixing ratios reach their peak in the first
365　five minutes, except for fire no. 12 (Engelmann spruce - duff), from which HONO

concentration remains nearly constant over the course of each fire, but much lower than HONO concentration of the rest of the fires. The largest HONO and HNO_3 were emitted from burning subalpine fir-Fish Lake canopy (fire no. 15), integrated concentration of up to 177 ppbv and 1.9 ppbv in the first 5-minute sample, respectively. We note that fires no. 12 has the smallest MCE value 0.868 (FIREX, 2016), and abnormal flow rate (less than half of the typical flow rate during all other measurements) due to the inlet filter clogging from extraordinarily large particulate loadings. In general, the closer the MCE value is to 1, the more likely N-oxidation (e.g. NO_x and HONO) dominates over N-reduction (e.g. NH_3 and HCN) as a result of flaming; when MCE approaches 0.8, more smoldering occurs such that N-reduction becomes dominant (Ferek et al., 1998; Goode et al., 1999; McMeeking et al., 2009; Yokelson et al., 1996, 2008). Accordingly, the smoldering combustion condition of fire no. 12 leads to lower concentration of oxidized nitrogen species than the rest of the fires in this study. Although fires no. 15 and no. 17 have relatively low MCE (~0.89), the pulse of HONO in first 5-10 minutes suggest an active flaming phase followed by longer smoldering phase. This indicates both fires had combustion conditions that consisted of a mixture of flaming and smoldering, and thus significant HONO was still produced. In addition, HONO/NO_x ratio ranged from 0.13 to 0.53 with a mean of 0.29±0.12 (1σ), comparable with previous results of laboratory experiments (0.11±0.04) and field experiments (0.23±0.09) (Akagi et al., 2013; Burling et al., 2010, 2011)

3.2 Verification of ADS collected HONO concentration
The HONO collected with the ADS represents a mean value over the course of each entire burn. We first compare HONO concentration recovered from the ADS, denoted as [HONO]$_{ADS}$, with that measured with the collocated MC/IC when both measurements were available (Fig. 2). The comparison demonstrates good consistency across all fires, with the [HONO]$_{ADS}$ of all available fires falling within the first and third quartile of MC/IC HONO data. Additionally, we made intercomparisons between [HONO]$_{ADS}$ with mean values of various high resolution methods including MC/IC, OP-FTIR, ACES and PTR-ToF that are also available from the NOAA data archive (Fig. 3; FIREX, 2016). The mean values used for the comparison are shown in Table S2. The linear regression results for all four comparisons are:

$$[HONO]_{ADS} = (1.07\pm0.24) \, [HONO]_{MCIC} - 0.72 \qquad \text{Eq. (1)}$$
$(R^2 = 0.63; \, p_{slope} < 0.001, \, p_{intercept}=0.95);$

$$[HONO]_{ADS} = (1.07\pm0.08) \, [HONO]_{ACES} - 4.63 \qquad \text{Eq. (2)}$$
$(R^2 = 0.95; \, p_{slope} < 1\times10^{-6}, \, p_{intercept}=0.32);$

$$[HONO]_{ADS} = (1.07\pm0.22) \, [HONO]_{FTIR} + 5.48 \qquad \text{Eq. (3)}$$
$(R^2 = 0.75; \, p_{slope} < 0.005, \, p_{intercept}=0.48);$

$$[HONO]_{ADS} = (1.08\pm0.19) \, [HONO]_{PTR-ToF} - 8.81 \qquad \text{Eq. (4)}$$
$(R^2 = 0.87; \, p_{slope} < 0.005, \, p_{intercept}=0.28).$

411 We found significant linear correlation between each of the [HONO] techniques and
412 [HONO] $_{ADS}$ with a slope of ~1. Note that the y-intercepts of Eq. (1)—(4) are much
413 smaller than the overall range of measured [HONO] (up to 121 ppbv). In addition, p-
414 values of the intercepts for all 4 fittings are much greater than 0.05, suggesting the
415 intercepts are not significantly different from zero. All data except one fall within 95%
416 prediction interval bounds of the overall fitting (Fig. 3). Therefore, we conclude that the
417 ADS method has high capture efficiency of HONO in the biomass combustion
418 environment, which assures the accuracy of the isotopic composition analysis and
419 applicability of this method for field-based biomass combustion research.
420
421 **3.3 Isotopic composition of HONO and NO$_x$ from burning different biomass**
422
423 δ^{15}N of NO$_x$ and HONO emitted from burning various biomass types in this study ranged
424 from -4.3 ‰ to +7.0‰ and -5.3 to +5.8‰, respectively (Table 1). There is no direct
425 dependence of δ^{15}N on concentration of either HONO or NO$_x$ (Figure S2). In Fig. 4, δ^{15}N
426 values of NO$_x$ and HONO are shown for each biomass type. Each value represents a
427 concentration-weighted mean (if multiple samples were collected for a biomass type)
428 with error bars representing propagation of replicate variation and method precision. For
429 biomass types burned in replicate (ponderosa pine, lodgepole pine, Engelmann spruce,
430 and Douglas-fir), the δ^{15}N-NO$_x$ and δ^{15}N-HONO variation within a given biomass type is
431 smaller than the full range across all fuel types. Additionally, we note that the variations
432 of δ^{15}N-NO$_x$ and δ^{15}N-HONO for ponderosa pine and δ^{15}N-HONO for Engelmann spruce
433 are larger than the method analytical precision of δ^{15}N-NO$_x$ (1.5‰) and δ^{15}N-HONO
434 (0.5‰), respectively, which represents fire-by-fire variation likely due to different
435 combustion conditions and/or different fuel compositions. For example, fuel moisture
436 content derived from the original biomass weight and dry biomass weight reveal that the
437 ponderosa pine burned in fire no.3 had more moisture content (48.1%) than fire no.2
438 (32.1%), which could affect combustion temperature and thus product formation. Fig. 4
439 also illustrates burning different biomass parts from specific vegetation can result in
440 fairly diverse δ^{15}N-HONO and δ^{15}N-NO$_x$, e.g. among ponderosa pine mixture, canopy
441 and litter, as well as between Engelmann spruce mixture and duff.
442
443 Our δ^{15}N-NO$_x$ range falls well within the range (-7‰ to +12‰) found in the FLAME-4
444 experiment (Fibiger and Hastings, 2016). The FLAME-4 study investigated NO$_x$
445 emissions from burning a relatively large range of vegetation biomass from all over the
446 world, and found a linear relationship (Eq. (5)), indicating that 83% of the variation of
447 δ^{15}N-NO$_x$ is explained by δ^{15}N-biomass. The biomass types burned in this work focused
448 on vegetation in the western U.S., and differ greatly from that in FLAME-4, with
449 Ponderosa pine being the only common biomass between the two studies. Specifically,
450 the δ^{15}N-biomass range (-4.2‰ to +0.9‰) for this work is much narrower than that of the
451 FLAME-4 experiment (-8‰ to +8‰).
452
453 δ^{15}N-NO$_x$ = 0.41 δ^{15}N-biomass + 1.0 (r^2=0.83, p<0.001)   Eq. (5)
454
455 To compare with the relationship found in Fibiger and Hastings (2016) we mass weighted
456 the contributions from different components of the same biomass type. For the same type

457   of biomass, δ^{15}N-biomass varies amongst different parts of the vegetation with
458   differences as great as 4.1‰, 2.4‰, 4.6‰ and 2.6‰ for ponderosa pine, lodgepole pine,
459   Douglas-fir and Engelmann spruce, respectively (Table S1). In the FIREX experiments,
460   many of the burns were conducted for mixtures of various vegetation parts. For instance,
461   one ponderosa pine fire contains canopy (~30%), litter (~28%), and other parts (~42%)
462   including duff and shrub, and the compositions vary slightly amongst each burn.
463   Therefore, the δ^{15}N of a particular biomass mixture is mass weighted according to its
464   composition contribution from each part (Table S1). Similarly, the δ^{15}N-NO$_x$ and δ^{15}N-
465   HONO from fires of different biomass parts are weighted by concentrations for each
466   biomass type, i.e. ponderosa pine (including mixture, canopy and litter) and Engelmann
467   spruce (including mixture and duff), to produce a signature associated with combustion
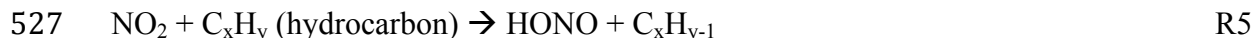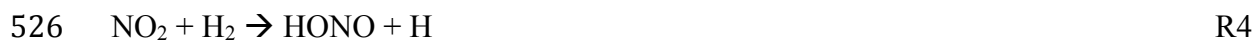468   of that biomass type.
469
470   For purpose of comparison among different biomass types, we average δ^{15}N-NO$_x$ (δ^{15}N-
471   HONO) weighted by concentrations for each biomass type, i.e. ponderosa pine (including
472   mixture, canopy and litter) and Engelmann spruce (including mixture and duff) (all data
473   are listed in Table S3). Linear regressions between δ^{15}N-HONO and δ^{15}N-biomass, as
474   well as that between δ^{15}N-NO$_x$ and δ^{15}N-biomass, show that both δ^{15}N-HONO and δ^{15}N-
475   NO$_x$ increase with δ^{15}N-biomass in general (Fig. S3). However, the linear regressions
476   performed here are limited by small datasets (4 data points each) and unsurprisingly yield
477   insignificant linear correlations for δ^{15}N-HONO (or δ^{15}N-NO$_x$) versus δ^{15}N-biomass (p
478   values are 0.1 and 0.5, respectively). Still, combining our results of δ^{15}N-NO$_x$ versus
479   δ^{15}N-biomass from this work with those from the FLAME-4 study (Fibiger and Hastings,
480   2016) results in a significant linear correlation (Eq. (6)) and is shown in Fig. 5. Despite
481   differences in burned biomass types between the two studies, our δ^{15}N-NO$_x$ reasonably
482   overlap with the FLAME-4 results within our δ^{15}N-biomass range. The relationship
483   between δ^{15}N-NO$_x$ and δ^{15}N-biomass (Eq. (6)) for the combined data highly reproduces
484   that obtained solely from FLAME-4 study (Eq. (5)) and confirms the dependence of
485   δ^{15}N-NO$_x$ on δ^{15}N-biomass.
486
487   δ^{15}N-NO$_x$ = (0.42±0.17) δ^{15}N-biomass + 1.3 (r^2=0.71, p<0.001)   Eq. (6)
488
489   The mean values weighted by concentration plotted in Fig. 4 show ^{15}N of HONO is
490   consistently slightly more depleted than that of NO$_x$ (δ^{15}N-HONO < δ^{15}N-NO$_x$) across all
491   the biomass types, except for ponderosa pine (litter) that results in an opposite
492   relationship between δ^{15}N-HONO and δ^{15}N-NO$_x$. Furthermore, δ^{15}N-HONO is linearly
493   correlated with δ^{15}N-NO$_x$ following a relationship of Eq. (7) within the δ^{15}N-NO$_x$ and
494   δ^{15}N-HONO range obtained in the current study (Fig. 6). This provides potential insights
495   into HONO-NO$_x$ interactions and HONO formation pathways in fresh emissions from
496   biomass burning. Although a number of studies on wildfire biomass burning have
497   suggested that partitioning of N emissions between NO$_x$ and NH$_3$ depends on combustion
498   conditions represented by MCE (Ferek et al., 1998; Goode et al., 1999; McMeeking et al.,
499   2009; Yokelson et al., 1996, 2008), HONO formation pathways remain unclear
500   (Alvarado et al., 2009, 2015; Nie et al., 2015).

501   δ^{15}N-HONO = 1.01 δ^{15}N-NO$_x$ - 1.52 (R^2 = 0.89, p<0.001)   Eq. (7)

502 Previous mechanistic studies on combustion of biomass/biofuel model compounds in a
503 well controlled closed system have investigated detailed nitrogen chemistry in the gas
504 phase, suggesting NO_x and HONO are formed from chain reactions involving oxidation
505 of precursors NH_3 and HCN, which are produced via devolatilization and pyrolysis of
506 amines and proteins in biomass/biofuel (Houshfar et al., 2012; Lucassen et al., 2011).
507 When the combustion conditions favor the oxidation of NH_3 and HCN, NO is first
508 formed and the chain reactions control the cycling of reactive nitrogen species (NO, NO_2
509 and HONO). Detailed and mechanistic nitrogen chemistry for the chemical relationship
510 between NO_x and HONO in the combustion environment have been discussed in earlier
511 works (Chai and Goldsmith, 2017; Shrestha et al., 2018; Skreiberg et al., 2004). In
512 addition, Houshfar et al. (2012) performed biomass combustion kinetic modeling with
513 reduced mechanism via sensitivity analysis. From these works, we extract major
514 pathways (R1-R11) that are likely responsible for fast gas-phase inter-conversion
515 between NO_x and HONO within the combustion system. They found that whether HONO
516 is preferably converted from NO or NO_2 in series during nitrogen transformation
517 (referred to as nitrogen flow) critically depends on temperature. Specifically, within 1
518 second of residence time, at moderate temperatures (e.g. 700 °C), preferable nitrogen
519 flow following NO formation in biomass combustion is NO→NO_2→HONO→NO, and
520 major reactions involving NO_x-HONO conversion are listed in R1-R6; at high
521 temperatures (e.g. 850 °C and above), the nitrogen flow cycle NO→HONO→NO_2→NO
522 becomes preferable, and major reactions involving NO_x-HONO are R7-R11.

523   NO_2 + HNOH → HONO + HNO   R1

524   NO_2 + HNO → HONO + NO   R2

525   NO_2 + HO_2 → HONO + O_2 R3

526   NO_2 + H_2 → HONO + H   R4

527   NO_2 + C_xH_y (hydrocarbon) → HONO + C_xH_{y-1} R5

528   HONO → OH + NO   R6

529   OH + NO → HONO   R7

530   HONO + NH_2 → NO_2 + NH_3 R8

531   HONO + NH → NO_2 + NH_2 R9

532   HONO + O → NO_2 + OH   R10

533   HONO + OH → NO_2 + H_2O R11

534 Although our studied fuels are more complicated in composition than a model system
535 involving no more than a few starting species, results from the above studies provide
536 fundamental underpinnings for biomass combustion. Also note that heterogeneous
537 chemistry after these species were emitted was not considered here as the residence time

538 of the fresh plume in our study was ~5 seconds, which is of the same magnitude as that
539 predicted in the nitrogen flow analysis (Houshfar et al., 2012). Kinetic isotope effects
540 (KIE) of these reactions have not been characterized; so only a semi-quantitative
541 prediction is presented here. At low temperatures, R1-R5 are all H-abstraction reactions
542 involving loose transition states that have significant activation energy; a primary KIE is
543 expected for such conditions and leads to ^{15}N depletion in the product (HONO) (Chai et
544 al., 2014; Matsson and Westaway, 1999, and references therein). Additionally, R6 is a
545 unimolecular dissociation reaction with no reaction barrier, and hence R6 could be
546 expected to have a small kinetic isotope effect enriching ^{15}N in HONO, somewhat
547 offsetting the depletion that arose from R1-R5. Consequently, the overall isotope effect of
548 R1-R6 would lead to δ^{15}N-HONO < δ^{15}N-NO$_x$ by a small difference, consistent with our
549 results (Fig. 4). On the other hand, the KIE for the reactions R7-R11 at higher
550 temperatures (> 850 °C) is expected to enrich ^{15}N in HONO relative to NO$_x$ (Chai and
551 Dibble, 2014), leading to an opposite isotope effect to that predicted at lower
552 temperatures.

553 Temperatures of the biomass combustion process span a large range involving different
554 processes including preheating, drying, distillation, pyrolysis, gasification (aka "glowing
555 combustion") and oxidation in turbulent diffusion flames at a range of temperatures
556 associated with changing flame dynamics (Yokelson et al., 1996). Despite this
557 complexity, our measured slight ^{15}N enrichment in NO$_x$ compared to HONO (Table 1,
558 Fig. 4) suggests that the reactions R1-R6 played a more important role than R7-R11 in
559 HONO formation during the FIREX Fire Lab experiments.

560
561 **3.4 Isotopic composition of nitrates collected on particle filters**
562 All Nylasorb filter extract solutions showed no detectable NO$_3^-$ and NO$_2^-$ concentrations,
563 indicating no significant amount of HNO$_3$ was collected on these filters, which is
564 consistent with the very low concentrations measured by MC/IC (note that low
565 concentration and limited sample volume also preclude further isotopic analysis of HNO$_3$
566 collected by MC/IC). By contrast, we found 5 out of 20 particulate filter extract solutions
567 had detectable NO$_3^-$ concentration that were sufficient (10 nmol N) for isotopic
568 composition analysis (Table 1). δ^{15}N and δ^{18}O reported here are considered to represent
569 NO$_3^-$(p). δ^{15}N-NO$_3^-$(p) of the five samples (burns) range from -10.6 to -7.4 ‰, all of
570 which are more ^{15}N depleted than that of HONO and NO$_x$. In addition, the smaller range
571 of δ^{15}N-NO$_3^-$ than that of δ^{15}N-HONO and δ^{15}N-NO$_x$ rules out possible transformation of
572 NO$_x$ and HONO to nitrate on the filters, which could distort the isotopic composition of
573 NO$_x$ and HONO.
574
575 In the FLAME-4 experiments, only one particulate filter had captured NO$_3^-$(p) above the
576 concentration detection limit, whereas HNO$_3$ collected on Nylasorb filters from 7
577 experiments were above the concentration detection limit and therefore only δ^{15}N-HNO$_3$
578 (-0.3‰ to 11.2‰) were reported (Fibiger and Hastings, 2016). The contrast with our
579 filter results are likely attributed to different formation mechanisms under different
580 conditions, in addition to variation of fuel types. Of the 7 detectable HNO$_3$ collections
581 from FLAME-4, 5 represented room burns for which samples were collected from smoke
582 aged for 1-2 hours in the lab, and the sampled HNO$_3$ was likely a secondary product. By

583   contrast all our observed $NO_3^-(p)$ were in fresh emissions and may have been derived
584   from plant nitrate (Cárdenas-Navarro et al., 1999) and/or combustion reactions. There
585   have been no other studies on $\delta^{15}N$ of $NO_3^-(p)$ and HNO_3 directly emitted from fresh
586   plumes to the best of our knowledge, so more investigation using both laboratory work
587   (isotope effect) and kinetic modeling will be needed in order to understand formation
588   mechanisms of HNO_3 and $NO_3^-(p)$ in the biomass combustion process and their
589   respective isotope effects.
590
591   In addition to $\delta^{15}N$, we report $\delta^{18}O$ of HONO and $NO_3^-(p)$ directly emitted from biomass
592   burning plumes with ranges of 5.2‰ to 15.2‰ and 11.5‰ to 14.8‰, respectively. These
593   are the first observations reported for $\delta^{18}O$ of reactive nitrogen species directly emitted
594   from biomass burning and low values are expected for the $\delta^{18}O$, which, in this case, is
595   mainly extracted from that of molecular oxygen ($\delta^{18}O$ = ~23.5‰) (Kroopnick and Craig,
596   1972), biomass/cellulose ($\delta^{18}O$ = 15‰–35‰), and/or biomass contained water ($\delta^{18}O$ =
597   ~ 0‰– 16‰) (Keel et al., 2016). In field studies where photochemistry and O_3 are
598   inevitably involved in the reactive nitrogen cycle in various stages of aged plumes, we
599   expect to see much more elevated $\delta^{18}O$ values of HONO and $NO_3^-(p)$ due to the
600   extremely high value of $\delta^{18}O$-O_3 (~110‰) (Vicars and Savarino, 2014). Therefore, the
601    $\delta^{18}O$ found in the lab is helpful in understanding conditions where photochemistry would
602   not apply (e.g. nighttime fresh smoke) and should be distinguishable from the expected
603   higher $\delta^{18}O$ that would be found in aged smoke and/or daytime fresh smoke.
604
605   **4 Conclusions**
606
607   In this study we applied new methods for characterizing the isotopic composition of
608   reactive nitrogen species including NO_x ($\delta^{15}N$), HONO ($\delta^{15}N$ and $\delta^{18}O$), and $NO_3^-(p)$
609   ($\delta^{15}N$ and $\delta^{18}O$) emitted directly from biomass burning. We measured fresh (stack)
610   emissions from 20 laboratory fires of different fuels during the 2016 FIREX Fire Lab
611   experiments. NO_x, HONO and HNO_3 emitted in fresh smoke reached their peak in most
612   of our fires within five minutes of ignition of biomass (i.e. when flaming combustion
613   peaked). The HONO mixing ratio was typically ~2 orders of magnitude larger than
614   HNO_3, and HONO/NO_x ratio ranged from 0.13 to 0.53.
615
616   Our HONO collection method (ADS) for isotopic analysis was applied to biomass
617   burning (BB) for the first time. The good agreement for concentration comparison
618   between our method and 4 high time-resolution HONO concentration methods suggests
619   high collection efficiency of HONO from BB emissions, which ensures accurate isotopic
620   compositional analysis. Comparison with concurrent observations and a previous study
621   show that the combination of our HONO and NO_x collection methods are compatible,
622   allowing for simultaneous determination of the isotopic composition of both HONO and
623   NO_x. This provides important potential for investigating the photochemical and non-
624   photochemical relationships between HONO and NO_x in a variety of environments, and
625   especially in BB plumes.
626
627    $\delta^{15}N$-NO_x emitted from burning various Western U.S. biomass types in this study ranged
628   from -4.3 ‰ to +7.0 ‰, falling well within the range found by Fibiger and Hastings

629   (2016), although the vegetation types were much broader in the earlier study. We report
630   the first δ^{15}N-HONO emitted directly from burning, ranging from -5.3‰ to +5.8‰. δ^{15}N-
631   NO_x and δ^{15}N-HONO range derived from BB can be further compared with that from
632   other sources using the same methods presented here, and provide insights into source
633   signatures for both NO_x and HONO. This study also showed the important capability of
634   determining δ^{18}O-HONO and δ^{18}O-NO_3^-(p) from BB plumes, and we expect δ^{18}O of both
635   HONO and NO_3^-(p) produced under photochemical conditions will be much higher than
636   the lab results due to the important role of O_3 in reactive nitrogen oxidation.
637
638   Interestingly, the linear correlation between δ^{15}N-HONO and δ^{15}N-NO_x for the biomass
639   we studied suggests systematic co-production of NO_x and HONO occurs during biomass
640   combustion and both of them are released as primary pollutants in fresh smoke. The
641   relationship between δ^{15}N-HONO and δ^{15}N-NO_x likely reflects that HONO was produced
642   to a larger extent at moderate combustion temperatures (< ~800 °C) than higher
643   temperatures on the basis of a simplified mechanism for flow of reactive nitrogen species.
644   However, we note that this relationship is derived from all measured δ^{15}N-HONO and
645   δ^{15}N-NO_x in fires ranging from smoldering to flaming, so is not necessarily
646   representative of a particular combustion condition. Still, it is likely that a compilation
647   over a range of conditions is more useful for potentially distinguishing HONO sources
648   and formation pathways in the environment since it will always be a challenge to assess
649   exact combustion temperatures. Determining these relationships in real wildfire smoke
650   will be essential for better constraint on NO_x and HONO budgets, and eventually may
651   improve ozone and secondary aerosol predictions for regional air quality.
652

653   *Data availability.* The data from the laboratory tests are available on request from the
654   corresponding authors. Data from the 2016 Missoula Fire lab are available here:
655   https://esrl.noaa.gov/csd/groups/csd7/measurements/2016firex/FireLab/DataDownload/

656   *Supplement.*

663   *Competing interests.* The authors declare that they have no conflicts of interest.

674 **References**
675

676 Akagi, S. K., Craven, J. S., Taylor, J. W., McMeeking, G. R., Yokelson, R. J., Burling, I.
677 R., Urbanski, S. P., Wold, C. E., Seinfeld, J. H., Coe, H., Alvarado, M. J. and Weise, D.
678 R.: Evolution of trace gases and particles emitted by a chaparral fire in California, Atmos
679 Chem Phys, 12(3), 1397–1421, doi:10.5194/acp-12-1397-2012, 2012.

680 Akagi, S. K., Yokelson, R. J., Burling, I. R., Meinardi, S., Simpson, I., Blake, D. R.,
681 McMeeking, G. R., Sullivan, A., Lee, T., Kreidenweis, S., Urbanski, S., Reardon, J.,
682 Griffith, D. W. T., Johnson, T. J. and Weise, D. R.: Measurements of reactive trace gases
683 and variable O3 formation rates in some South Carolina biomass burning plumes, Atmos
684 Chem Phys, 13(3), 1141–1165, doi:10.5194/acp-13-1141-2013, 2013.

685 Alvarado, M. J. and Prinn, R. G.: Formation of ozone and growth of aerosols in young
686 smoke plumes from biomass burning: 1. Lagrangian parcel studies, J. Geophys. Res.
687 Atmospheres, 114(D9), doi:10.1029/2008JD011144, 2009.

688 Alvarado, M. J., Wang, C. and Prinn, R. G.: Formation of ozone and growth of aerosols
689 in young smoke plumes from biomass burning: 2. Three-dimensional Eulerian studies, J.
690 Geophys. Res. Atmospheres, 114(D9), doi:10.1029/2008JD011186, 2009.

691 Alvarado, M. J., Lonsdale, C. R., Yokelson, R. J., Akagi, S. K., Coe, H., Craven, J. S.,
692 Fischer, E. V., McMeeking, G. R., Seinfeld, J. H., Soni, T., Taylor, J. W., Weise, D. R.
693 and Wold, C. E.: Investigating the links between ozone and organic aerosol chemistry in
694 a biomass burning plume from a prescribed fire in California chaparral, Atmos Chem
695 Phys, 15(12), 6667–6688, doi:10.5194/acp-15-6667-2015, 2015.

696 Böhlke, J. K., Mroczkowski, S. J. and Coplen, T. B.: Oxygen isotopes in nitrate: new
697 reference materials for 18O:17O:16O measurements and observations on nitrate-water
698 equilibration, Rapid Commun. Mass Spectrom., 17(16), 1835–1846,
699 doi:10.1002/rcm.1123, 2003.

700 Burling, I. R., Yokelson, R. J., Griffith, D. W. T., Johnson, T. J., Veres, P., Roberts, J.
701 M., Warneke, C., Urbanski, S. P., Reardon, J., Weise, D. R., Hao, W. M. and de Gouw,
702 J.: Laboratory measurements of trace gas emissions from biomass burning of fuel types
703 from the southeastern and southwestern United States, Atmos Chem Phys, 10(22),
704 11115–11130, doi:10.5194/acp-10-11115-2010, 2010.

705 Burling, I. R., Yokelson, R. J., Akagi, S. K., Urbanski, S. P., Wold, C. E., Griffith, D. W.
706 T., Johnson, T. J., Reardon, J. and Weise, D. R.: Airborne and ground-based
707 measurements of the trace gases and particles emitted by prescribed fires in the United
708 States, Atmos Chem Phys, 11(23), 12197–12216, doi:10.5194/acp-11-12197-2011, 2011.

709 Cárdenas-Navarro, R., Adamowicz, S. and Robin, P.: Nitrate accumulation in plants: a
710 role for water, J. Exp. Bot., 50(334), 613–624, doi:10.1093/jxb/50.334.613, 1999.

711 Casciotti, K. L., Sigman, D. M., Hastings, M. G., Böhlke, J. K. and Hilkert, A.:
712 Measurement of the Oxygen Isotopic Composition of Nitrate in Seawater and Freshwater
713 Using the Denitrifier Method, Anal. Chem., 74(19), 4905–4912, doi:10.1021/ac020113w,
714 2002.

715 Casciotti, K. L., Böhlke, J. K., McIlvin, M. R., Mroczkowski, S. J. and Hannon, J. E.:
716 Oxygen Isotopes in Nitrite: Analysis, Calibration, and Equilibration, Anal. Chem., 79(6),
717 2427–2436, doi:10.1021/ac061598h, 2007.

718 Chai, J. and Dibble, T. S.: Pressure Dependence and Kinetic Isotope Effects in the
719 Absolute Rate Constant for Methoxy Radical Reacting with NO2, Int. J. Chem. Kinet.,
720 46(9), 501–511, doi:10.1002/kin.20865, 2014.

721 Chai, J. and Goldsmith, C. F.: Rate coefficients for fuel + NO2: Predictive kinetics for
722 HONO and HNO2 formation, Proc. Combust. Inst., 36(1), 617–626,
723 doi:10.1016/j.proci.2016.06.133, 2017.

724 Chai, J. and Hastings, M.: Collection Method for Isotopic Analysis of Gaseous Nitrous
725 Acid, Anal. Chem., 90(1), 830–838, doi:10.1021/acs.analchem.7b03561, 2018.

726 Chai, J., Hu, H., Dibble, T. S., Tyndall, G. S. and Orlando, J. J.: Rate Constants and
727 Kinetic Isotope Effects for Methoxy Radical Reacting with NO2 and O2, J. Phys. Chem.
728 A, 118(20), 3552–3563 [online] Available from:
729 http://pubs.acs.org/doi/abs/10.1021/jp501205d (Accessed 24 June 2015), 2014.

730 Christian, T. J., Kleiss, B., Yokelson, R. J., Holzinger, R., Crutzen, P. J., Hao, W. M.,
731 Shirai, T. and Blake, D. R.: Comprehensive laboratory measurements of biomass-burning
732 emissions: 2. First intercomparison of open-path FTIR, PTR-MS, and GC-MS/FID/ECD,
733 J. Geophys. Res. Atmospheres, 109(D2), doi:10.1029/2003JD003874, 2004.

734 Cook, P. A., Savage, N. H., Turquety, S., Carver, G. D., O'Connor, F. M., Heckel, A.,
735 Stewart, D., Whalley, L. K., Parker, A. E., Schlager, H., Singh, H. B., Avery, M. A.,
736 Sachse, G. W., Brune, W., Richter, A., Burrows, J. P., Purvis, R., Lewis, A. C., Reeves,
737 C. E., Monks, P. S., Levine, J. G. and Pyle, J. A.: Forest fire plumes over the North
738 Atlantic: p-TOMCAT model simulations with aircraft and satellite measurements from
739 the ITOP/ICARTT campaign, J. Geophys. Res. Atmospheres, 112, D10S43,
740 doi:10.1029/2006JD007563, 2007.

741 Crutzen, P. J. and Andreae, M. O.: Biomass burning in the tropics: impact on atmospheric
742 chemistry and biogeochemical cycles, Science, 250(4988), 1669–1678,
743 doi:10.1126/science.250.4988.1669, 1990.

744 Dibb, J. E., Arsenault, M., Peterson, M. C. and Honrath, R. E.: Fast nitrogen oxide
745 photochemistry in Summit, Greenland snow, Atmos. Environ., 36(15–16), 2501–2511,
746 doi:10.1016/S1352-2310(02)00130-9, 2002.

747   Ferek, R., Reid, J., Hobbs, P., Blake, D. and Liousse, C.: Emission factors of
748   hydrocarbons, halocarbons, trace gases and particles from biomass burning in Brazil, J.
749   Geophys. Res.-ATMOSPHERES, 103, 32107–32118, doi:10.1029/98JD00692, 1998.

750   Fibiger, D. L. and Hastings, M. G.: First Measurements of the Nitrogen Isotopic
751   Composition of NOx from Biomass Burning, Environ. Sci. Technol., 50(21), 11569–
752   11574, doi:10.1021/acs.est.6b03510, 2016.

753   Fibiger, D. L., Hastings, M. G., Lew, A. F. and Peltier, R. E.: Collection of NO and NO2
754   for Isotopic Analysis of NOx Emissions, Anal. Chem., 86(24), 12115–12121,
755   doi:10.1021/ac502968e, 2014.

756   FIREX: FIREX 2016 Fire Lab Data Archive, [online] Available from:
757   https://esrl.noaa.gov/csd/groups/csd7/measurements/2016firex/FireLab/DataDownload/in
758   dex.php?page=/csd/groups/csd7/measurements/2016firex/FireLab/DataDownload/
759   (Accessed 25 March 2019), 2016.

760   Goode, J. G., Yokelson, R. J., Susott, R. A. and Ward, D. E.: Trace gas emissions from
761   laboratory biomass fires measured by open-path Fourier transform infrared spectroscopy:
762   Fires in grass and surface fuels, J. Geophys. Res., 104, 21, doi:10.1029/1999JD900360,
763   1999.

764   Hastings, M. G., Casciotti, K. L. and Elliott, E. M.: Stable Isotopes as Tracers of
765   Anthropogenic Nitrogen Sources, Deposition, and Impacts, Elements, 9(5), 339–344,
766   doi:10.2113/gselements.9.5.339, 2013.

767   Houshfar, E., Skreiberg, Ø., Glarborg, P. and Løvås, T.: Reduced chemical kinetic
768   mechanisms for NO_x emission prediction in biomass combustion, Int. J. Chem. Kinet.,
769   4(44), 219–231, doi:10.1002/kin.20716, 2012.

770   Jaeglé, L., Steinberger, L., Martin, R. V. and Chance, K.: Global partitioning of NOx
771   sources using satellite observations: relative roles of fossil fuel combustion, biomass
772   burning and soil emissions, Faraday Discuss., 130, 407–423; discussion 491-517, 519–
773   524, 2005.

774   Jaffe, D. and Briggs, N.: Ozone production from wildfires: A critical review, Atmos.
775   Environ., 51, 1–10, doi:10.1016/j.atmosenv.2011.11.063, 2012.

776   Keel, S. G., Joos, F., Spahni, R., Saurer, M., Weigt, R. B. and Klesse, S.: Simulating
777   oxygen isotope ratios in tree ring cellulose using a dynamic global vegetation model,
778   Biogeosciences, 13(13), 3869–3886, doi:https://doi.org/10.5194/bg-13-3869-2016, 2016.

779   Keene, W. C., Lobert, J. M., Crutzen, P. J., Maben, J. R., Scharffe, D. H., Landmann, T.,
780   Hély, C. and Brain, C.: Emissions of major gaseous and particulate species during
781   experimental burns of southern African biomass, J. Geophys. Res. Atmospheres,
782   111(D4), doi:10.1029/2005JD006319, 2006.

783 Koss, A. R., Sekimoto, K., Gilman, J. B., Selimovic, V., Coggon, M. M., Zarzana, K. J.,
784 Yuan, B., Lerner, B. M., Brown, S. S., Jimenez, J. L., Krechmer, J., Roberts, J. M.,
785 Warneke, C., Yokelson, R. J. and Gouw, J. de: Non-methane organic gas emissions from
786 biomass burning: identification, quantification, and emission factors from PTR-ToF
787 during the FIREX 2016 laboratory experiment, Atmospheric Chem. Phys., 18(5), 3299–
788 3319, doi:https://doi.org/10.5194/acp-18-3299-2018, 2018.

789 Kraus, S.: DOASIS: a framework design for DOAS., 2006.

790 Kroopnick, P. and Craig, H.: Atmospheric oxygen: isotopic composition and solubility
791 fractionation, Science, 175(4017), 54–55, doi:10.1126/science.175.4017.54, 1972.

792 Lapina, K., Honrath R. E., Owen R. C., Val Martín M., Hyer E. J. and Fialho P.: Late
793 summer changes in burning conditions in the boreal regions and their implications for
794 NOx and CO emissions from boreal fires, J. Geophys. Res. Atmospheres, 113(D11),
795 doi:10.1029/2007JD009421, 2008.

796 Liu, X., Zhang, Y., Huey, L. G., Yokelson, R. J., Wang, Y., Jimenez, J. L., Campuzano-
797 Jost, P., Beyersdorf, A. J., Blake, D. R., Choi, Y., Clair, J. M. S., Crounse, J. D., Day, D.
798 A., Diskin, G. S., Fried, A., Hall, S. R., Hanisco, T. F., King, L. E., Meinardi, S.,
799 Mikoviny, T., Palm, B. B., Peischl, J., Perring, A. E., Pollack, I. B., Ryerson, T. B.,
800 Sachse, G., Schwarz, J. P., Simpson, I. J., Tanner, D. J., Thornhill, K. L., Ullmann, K.,
801 Weber, R. J., Wennberg, P. O., Wisthaler, A., Wolfe, G. M. and Ziemba, L. D.:
802 Agricultural fires in the southeastern U.S. during SEAC4RS: Emissions of trace gases
803 and particles and evolution of ozone, reactive nitrogen, and organic aerosol, J. Geophys.
804 Res. Atmospheres, 121(12), 7383–7414, doi:10.1002/2016JD025040, 2016.

805 Lucassen, A., Labbe, N., Westmoreland, P. R. and Kohse-Höinghaus, K.: Combustion
806 chemistry and fuel-nitrogen conversion in a laminar premixed flame of morpholine as a
807 model biofuel, Combust. Flame, 158(9), 1647–1666,
808 doi:10.1016/j.combustflame.2011.02.010, 2011.

809 Matsson, O. and Westaway, K. C.: Secondary Deuterium Kinetic Isotope Effects and
810 Transition State Structure, in Advances in Physical Organic Chemistry, vol. 31, edited by
811 D. Bethell, pp. 143–248, Academic Press., 1999.

812 McMeeking, G. R., Kreidenweis, S. M., Baker, S., Carrico, C. M., Chow, J. C., Collett, J.
813 L., Hao, W. M., Holden, A. S., Kirchstetter, T. W., Malm, W. C., Moosmüller, H.,
814 Sullivan, A. P. and Wold, C. E.: Emissions of trace gases and aerosols during the open
815 combustion of biomass in the laboratory, J. Geophys. Res. Atmospheres, 114(D19),
816 D19210, doi:10.1029/2009JD011836, 2009.

817 Miller, D. J., Wojtal, P. K., Clark, S. C. and Hastings, M. G.: Vehicle NOx emission
818 plume isotopic signatures: Spatial variability across the eastern United States, J. Geophys.
819 Res. Atmospheres, 122(8), 4698–4717, doi:10.1002/2016JD025877, 2017.

820　Miller, D. J., Chai, J., Guo, F., Dell, C. J., Karsten, H. and Hastings, M. G.: Isotopic
821　Composition of In Situ Soil NOx Emissions in Manure-Fertilized Cropland, Geophys.
822　Res. Lett., 45(21), 12,058-12,066, doi:10.1029/2018GL079619, 2018.

823　Min, K.-E., Washenfelder, R. A., Dubé, W. P., Langford, A. O., Edwards, P. M.,
824　Zarzana, K. J., Stutz, J., Lu, K., Rohrer, F., Zhang, Y. and Brown, S. S.: A broadband
825　cavity enhanced absorption spectrometer for aircraft measurements of glyoxal,
826　methylglyoxal, nitrous acid, nitrogen dioxide, and water vapor, Atmospheric Meas.
827　Tech., 9(2), 423–440, doi:https://doi.org/10.5194/amt-9-423-2016, 2016.

828　Neuman, J. A., Trainer, M., Brown, S. S., Min, K.-E., Nowak, J. B., Parrish, D. D.,
829　Peischl, J., Pollack, I. B., Roberts, J. M., Ryerson, T. B. and Veres, P. R.: HONO
830　emission and production determined from airborne measurements over the Southeast
831　U.S., J. Geophys. Res. Atmospheres, 121(15), 9237–9250, doi:10.1002/2016JD025197,
832　2016.

833　Nie, W., Ding, A. J., Xie, Y. N., Xu, Z., Mao, H., Kerminen, V.-M., Zheng, L. F., Qi, X.
834　M., Huang, X., Yang, X.-Q., Sun, J. N., Herrmann, E., Petäjä, T., Kulmala, M. and Fu, C.
835　B.: Influence of biomass burning plumes on HONO chemistry in eastern China, Atmos
836　Chem Phys, 15(3), 1147–1159, doi:10.5194/acp-15-1147-2015, 2015.

837　Perrino, C., De Santis, F. and Febo, A.: Criteria for the choice of a denuder sampling
838　technique devoted to the measurement of atmospheric nirous and nitric acids,
839　Atmospheric Environ. Part Gen. Top., 24(3), 617–626, doi:10.1016/0960-
840　1686(90)90017-H, 1990.

841　Pinto, J. P., Dibb, J., Lee, B. H., Rappenglück, B., Wood, E. C., Levy, M., Zhang, R.-Y.,
842　Lefer, B., Ren, X.-R., Stutz, J., Tsai, C., Ackermann, L., Golovko, J., Herndon, S. C.,
843　Oakes, M., Meng, Q.-Y., Munger, J. W., Zahniser, M. and Zheng, J.: Intercomparison of
844　field measurements of nitrous acid (HONO) during the SHARP campaign, J. Geophys.
845　Res. Atmospheres, 119(9), 5583–5601, doi:10.1002/2013JD020287, 2014.

846　Reinhardt, E. D., Keane, R. E. and Brown, J. K.: First Order Fire Effects Model: FOFEM
847　4.0, user's guide, Gen Tech Rep INT-GTR-344 Ogden UT US Dep. Agric. For. Serv.
848　Intermt. Res. Stn. 65 P, 344, doi:10.2737/INT-GTR-344, 1997.

849　Roberts, J. M., Veres, P., Warneke, C., Neuman, J. A., Washenfelder, R. A., Brown, S.
850　S., Baasandorj, M., Burkholder, J. B., Burling, I. R., Johnson, T. J., Yokelson, R. J. and
851　de Gouw, J.: Measurement of HONO, HNCO, and other inorganic acids by negative-ion
852　proton-transfer chemical-ionization mass spectrometry (NI-PT-CIMS): application to
853　biomass burning emissions, Atmos Meas Tech, 3(4), 981–990, doi:10.5194/amt-3-981-
854　2010, 2010.

855　Scheuer, E., Talbot, R. W., Dibb, J. E., Seid, G. K., DeBell, L. and Lefer, B.: Seasonal
856　distributions of fine aerosol sulfate in the North American Arctic basin during TOPSE, J.
857　Geophys. Res. Atmospheres, 108(D4), doi:10.1029/2001JD001364, 2003.

858   Selimovic, V., Yokelson, R. J., Warneke, C., Roberts, J. M., de Gouw, J., Reardon, J. and
859   Griffith, D. W. T.: Aerosol optical properties and trace gas emissions by PAX and OP-
860   FTIR for laboratory-simulated western US wildfires during FIREX, Atmos Chem Phys,
861   18(4), 2929–2948, doi:10.5194/acp-18-2929-2018, 2018.

862   Shrestha, K. P., Seidel, L., Zeuch, T. and Mauss, F.: Detailed Kinetic Mechanism for the
863   Oxidation of Ammonia Including the Formation and Reduction of Nitrogen Oxides,
864   Energy Fuels, doi:10.1021/acs.energyfuels.8b01056, 2018.

865   Sigman, D. M., Casciotti, K. L., Andreani, M., Barford, C., Galanter, M. and Böhlke, J.
866   K.: A Bacterial Method for the Nitrogen Isotopic Analysis of Nitrate in Seawater and
867   Freshwater, Anal. Chem., 73(17), 4145–4153, doi:10.1021/ac010088e, 2001.

868   Skreiberg, Ø., Kilpinen, P. and Glarborg, P.: Ammonia chemistry below 1400 K under
869   fuel-rich conditions in a flow reactor, Combust. Flame, 136(4), 501–518,
870   doi:10.1016/j.combustflame.2003.12.008, 2004.

871   Stockwell, C. E., Yokelson, R. J., Kreidenweis, S. M., Robinson, A. L., DeMott, P. J.,
872   Sullivan, R. C., Reardon, J., Ryan, K. C., Griffith, D. W. T. and Stevens, L.: Trace gas
873   emissions from combustion of peat, crop residue, domestic biofuels, grasses, and other
874   fuels: configuration and Fourier transform infrared (FTIR) component of the fourth Fire
875   Lab at Missoula Experiment (FLAME-4), Atmos Chem Phys, 14(18), 9727–9754,
876   doi:10.5194/acp-14-9727-2014, 2014.

877   Stutz, J., Oh, H.-J., Whitlow, S. I., Anderson, C., Dibb, J. E., Flynn, J. H., Rappenglück,
878   B. and Lefer, B.: Simultaneous DOAS and mist-chamber IC measurements of HONO in
879   Houston, TX, Atmos. Environ., 44(33), 4090–4098, doi:10.1016/j.atmosenv.2009.02.003,
880   2010.

881   Tkacik, D. S., Robinson, E. S., Ahern, A., Saleh, R., Stockwell, C., Veres, P., Simpson, I.
882   J., Meinardi, S., Blake, D. R., Yokelson, R. J., Presto, A. A., Sullivan, R. C., Donahue, N.
883   M. and Robinson, A. L.: A dual-chamber method for quantifying the effects of
884   atmospheric perturbations on secondary organic aerosol formation from biomass burning
885   emissions, J. Geophys. Res. Atmospheres, 122(11), 6043–6058,
886   doi:10.1002/2016JD025784, 2017.

887   Travis, K. R., Jacob, D. J., Fisher, J. A., Kim, P. S., Marais, E. A., Zhu, L., Yu, K.,
888   Miller, C. C., Yantosca, R. M., Sulprizio, M. P., Thompson, A. M., Wennberg, P. O.,
889   Crounse, J. D., St. Clair, J. M., Cohen, R. C., Laughner, J. L., Dibb, J. E., Hall, S. R.,
890   Ullmann, K., Wolfe, G. M., Pollack, I. B., Peischl, J., Neuman, J. A. and Zhou, X.: Why
891   do models overestimate surface ozone in the Southeast United States?, Atmos Chem
892   Phys, 16(21), 13561–13577, doi:10.5194/acp-16-13561-2016, 2016.

893   Trentmann, J., Yokelson, R. J., Hobbs, P. V., Winterrath, T., Christian, T. J., Andreae, M.
894   O. and Mason, S. A.: An analysis of the chemical processes in the smoke plume from a
895   savanna fire, J. Geophys. Res. Atmospheres, 110(D12), doi:10.1029/2004JD005628,
896   2005.

897 Val Martín, M., Honrath, R. E., Owen, R. C., Pfister, G., Fialho, P. and Barata, F.:
898 Significant enhancements of nitrogen oxides, black carbon, and ozone in the North
899 Atlantic lower free troposphere resulting from North American boreal wildfires, J.
900 Geophys. Res. Atmospheres, 111(D23), doi:10.1029/2006JD007530, 2006.

901 Veres, P., Roberts, J. M., Burling, I. R., Warneke, C., Gouw, J. de and Yokelson, R. J.:
902 Measurements of gas-phase inorganic and organic acids from biomass fires by negative-
903 ion proton-transfer chemical-ionization mass spectrometry, J. Geophys. Res.
904 Atmospheres, 115(D23), doi:10.1029/2010JD014033, 2010.

905 Vicars, W. C. and Savarino, J.: Quantitative constraints on the 17O-excess (Δ17O)
906 signature of surface ozone: Ambient measurements from 50°N to 50°S using the nitrite-
907 coated filter technique, Geochim. Cosmochim. Acta, 135(Supplement C), 270–287,
908 doi:10.1016/j.gca.2014.03.023, 2014.

909 Wojtal, P. K., Miller, D. J., O'Conner, M., Clark, S. C. and Hastings, M. G.: Automated,
910 High-resolution Mobile Collection System for the Nitrogen Isotopic Analysis of NOx, J.
911 Vis. Exp. JoVE, (118), doi:10.3791/54962, 2016.

912 Ye, C., Zhou, X., Pu, D., Stutz, J., Festa, J., Spolaor, M., Tsai, C., Cantrell, C., Mauldin,
913 R. L., Campos, T., Weinheimer, A., Hornbrook, R. S., Apel, E. C., Guenther, A., Kaser,
914 L., Yuan, B., Karl, T., Haggerty, J., Hall, S., Ullmann, K., Smith, J. N., Ortega, J. and
915 Knote, C.: Rapid cycling of reactive nitrogen in the marine boundary layer, Nature,
916 532(7600), 489–491, doi:10.1038/nature17195, 2016.

917 Yokelson, R., W. T. Griffith, D. and Ward, D.: Open-path Fourier transform infrared
918 studies of large-scale laboratory biomass fires, J. Geophys. Res., 101, 21067,
919 doi:10.1029/96JD01800, 1996.

920 Yokelson, R. J., Karl, T., Artaxo, P., Blake, D. R., Christian, T. J., Griffith, D. W. T.,
921 Guenther, A. and Hao, W. M.: The Tropical Forest and Fire Emissions Experiment:
922 overview and airborne fire emission factor measurements, Atmos Chem Phys, 7(19),
923 5175–5196, doi:10.5194/acp-7-5175-2007, 2007.

924 Yokelson, R. J., Christian, T. J., Karl, T. G. and Guenther, A.: The tropical forest and fire
925 emissions experiment: laboratory fire measurements and synthesis of campaign data,
926 Atmos Chem Phys, 8(13), 3509–3527, doi:10.5194/acp-8-3509-2008, 2008.

927 Yokelson, R. J., Crounse, J. D., DeCarlo, P. F., Karl, T., Urbanski, S., Atlas, E., Campos,
928 T., Shinozuka, Y., Kapustin, V., Clarke, A. D., Weinheimer, A., Knapp, D. J., Montzka,
929 D. D., Holloway, J., Weibring, P., Flocke, F., Zheng, W., Toohey, D., Wennberg, P. O.,
930 Wiedinmyer, C., Mauldin, L., Fried, A., Richter, D., Walega, J., Jimenez, J. L., Adachi,
931 K., Buseck, P. R., Hall, S. R. and Shetter, R.: Emissions from biomass burning in the
932 Yucatan, Atmos Chem Phys, 9(15), 5785–5812, doi:10.5194/acp-9-5785-2009, 2009.

933 Yuan, B., Koss, A., Warneke, C., Gilman, J. B., Lerner, B. M., Stark, H. and Gouw, J. A.
934 de: A high-resolution time-of-flight chemical ionization mass spectrometer utilizing
935 hydronium ions (H$_3$O$^+$ ToF-CIMS) for measurements of volatile organic compounds in

936   the atmosphere, Atmospheric Meas. Tech., 9(6), 2735–2752,
937   doi:https://doi.org/10.5194/amt-9-2735-2016, 2016.

938   Zarzana, K. J., Selimovic, V., Koss, A. R., Sekimoto, K., Coggon, M. M., Yuan, B.,
939   Dubé, W. P., Yokelson, R. J., Warneke, C., Gouw, J. A. de, Roberts, J. M. and Brown, S.
940   S.: Primary emissions of glyoxal and methylglyoxal from laboratory measurements of
941   open biomass burning, Atmospheric Chem. Phys., 18(20), 15451–15470,
942   doi:https://doi.org/10.5194/acp-18-15451-2018, 2018.

943   Zhou, S., Young, C. J., VandenBoer, T. C., Kowal, S. F. and Kahan, T. F.: Time-
944   Resolved Measurements of Nitric Oxide, Nitrogen Dioxide, and Nitrous Acid in an
945   Occupied New York Home, Environ. Sci. Technol., 52(15), 8355–8364,
946   doi:10.1021/acs.est.8b01792, 2018.

947
948
949
950
951
952
953
954
955
956
957
958
959
960
961
962
963
964
965
966
967
968
969
970
971
972
973
974
975
976
977
978
979

Table 1. Concentration (mean, derived from solution concentration and flow rate) and N isotopic composition for various biomass burning experiments, unit for all δ denotations is ‰. MCE values are extracted from NOAA FIREX fire archive. Note: fire no. 1, 7 and 13 were missing due to technical issues; NO_x results are only shown when blank/sample ratio is <70%. Biomass acronyms are defined in Sect. 2.1; in addition, d—duff, c—canopy, l-litter.

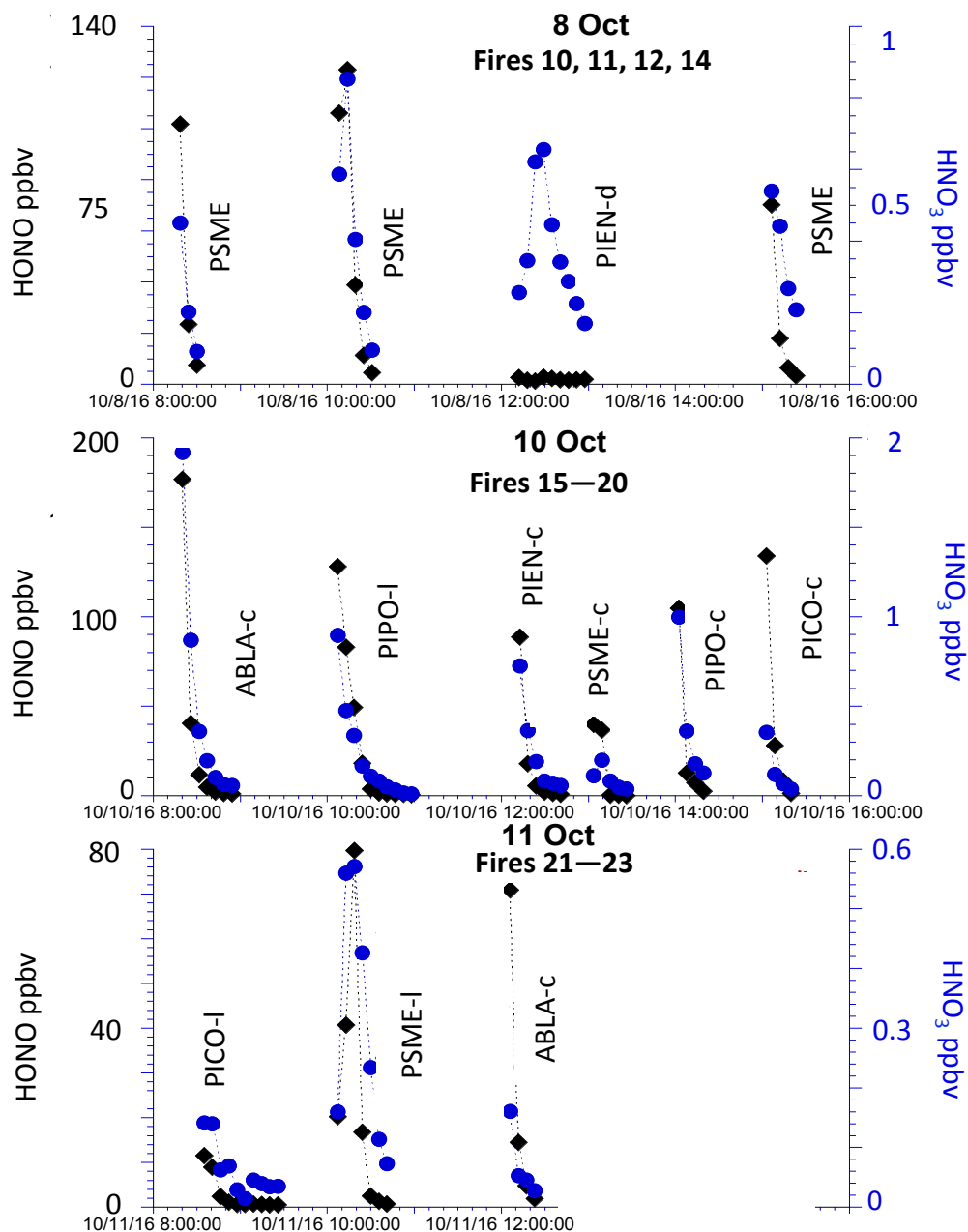| Biomass	Fire no.	HONO (ppbv)	$\delta^{15}N$-HONO	$\delta^{18}O$-HONO	NO_x (ppbv)	$\delta^{15}N$-NO_x	$\delta^{15}N$-biomass	$\delta^{15}N$-p-NO_3^-	$\delta^{18}O$-p-NO_3^-	HONO/NO_x	MCE
PIPO	2	19.9	-5.3	12.6	147.9	-1.1	0.3	-7.5	14.3	0.13	0.93
PIPO	3	35.8	1.7	11.6	124.7	2.3	0.3			0.29	0.94
PIPO	4	152.9	-3.1	10.6	716.8	-3.6	0.3			0.21	0.93
PICO	5	74.8	-2.3	8.8	170.8	-1.1	-3.4	-7.4	14.8	0.44	0.93
PICO	6	17.6	-1.9	8.4	94.7	1.4	-3.4			0.19	0.94
PIEN	8	25.7	-1.7	14.6	91.7	0.1	-2.4			0.28	0.92
PIEN	9	21.3	-4.8	9.5	73.6	-1.3	-2.8			0.29	0.93
PSME	10	42.2	-0.5	5.2	229.7	1.9	-1.4	-10.6	14.5	0.18	0.94
PSME	11	112.3	-0.4	15.2	571.8	3.3	-2.0			0.20	0.95
PIEN-d	12	17.1	-4.6	8.5	36.2	-4.3	-1.4	-9.9	11.5	0.47	0.87
PSME	14	25.3	0.1	14.9	70.0	2.1	-1.9			0.36	0.93
ABLA-c	15	51.0	2.1	9.9	95.5	3.4	-2.6	-8.9	12.7	0.53	0.89
PIPO-l	16	70.0	5.8	7.5	443.3	5.2	0.9			0.16	0.95
PIEN-c	17	47.1	6.1	14.8			-3.5				0.89
PSME-c	18	45.3	2.5	14.0			-1.4				0.93
PIPO-c	19	23.8	5.3	14.8	73.3	7.0	-0.1			0.32	0.93
PICO-c	20	52.5	3.0	14.9			-3.1				0.94
PICO-l	21	9.9	0.3	15.2			-4.2				0.93
PSME-l	22	40.0	1.9	10.2			-2.3				0.95
ABLA-c	23	40.8	0.5	12.2			-2.6				0.95

984
985

986
987 **Figure 1.** Temporal profile of HONO (black diamond) and HNO_3 (blue circle)
988 concentration measured using MC/IC method for various stack fires (fire numbers are
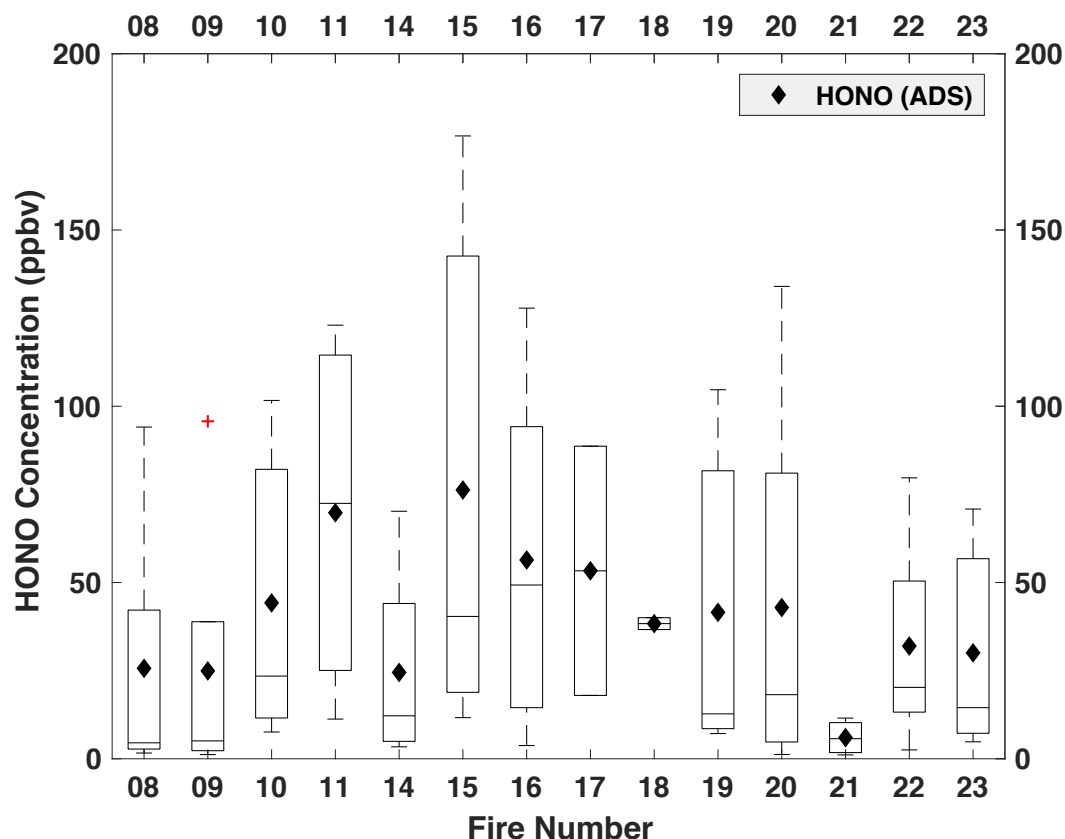989 referred to Table 1).

990
991

992
Figure 2. Box plot of MC/IC HONO measurement with 5 minutes resolution over the
course of each fire. Each box whisker represents 5th, 25th, 50th, 75th, 95th percentile of
HONO concentration during each collection period. Black diamond is the mean HONO
concentration recovered from ADS collection. The red cross symbolize outliers. Note no
isotopic analysis was performed for fire no. 12 (shown in Figure 1) due to insufficient
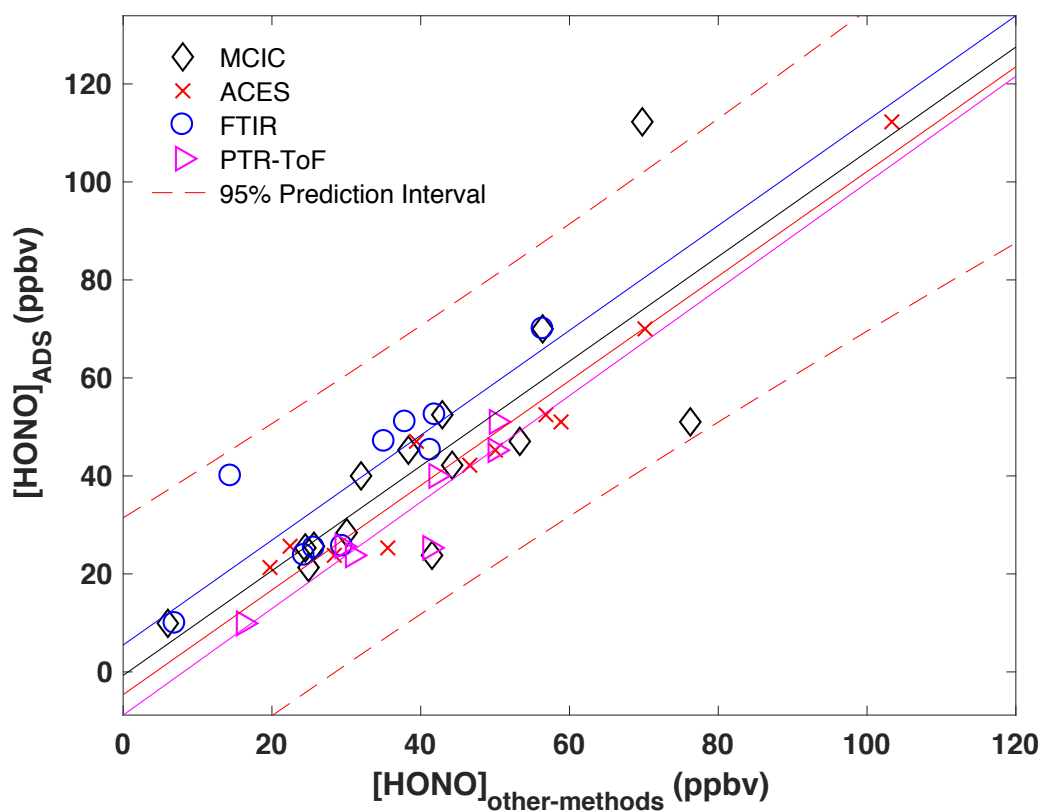amount of collected nitrite.

999
1000

Figure 3. Comparison of ADS measured HONO concentration with mean values of various high resolution methods including MC/IC, FTIR, ACES and PTR-ToF for available fires. Solid lines are linear regression of each dataset with the same symbol color.
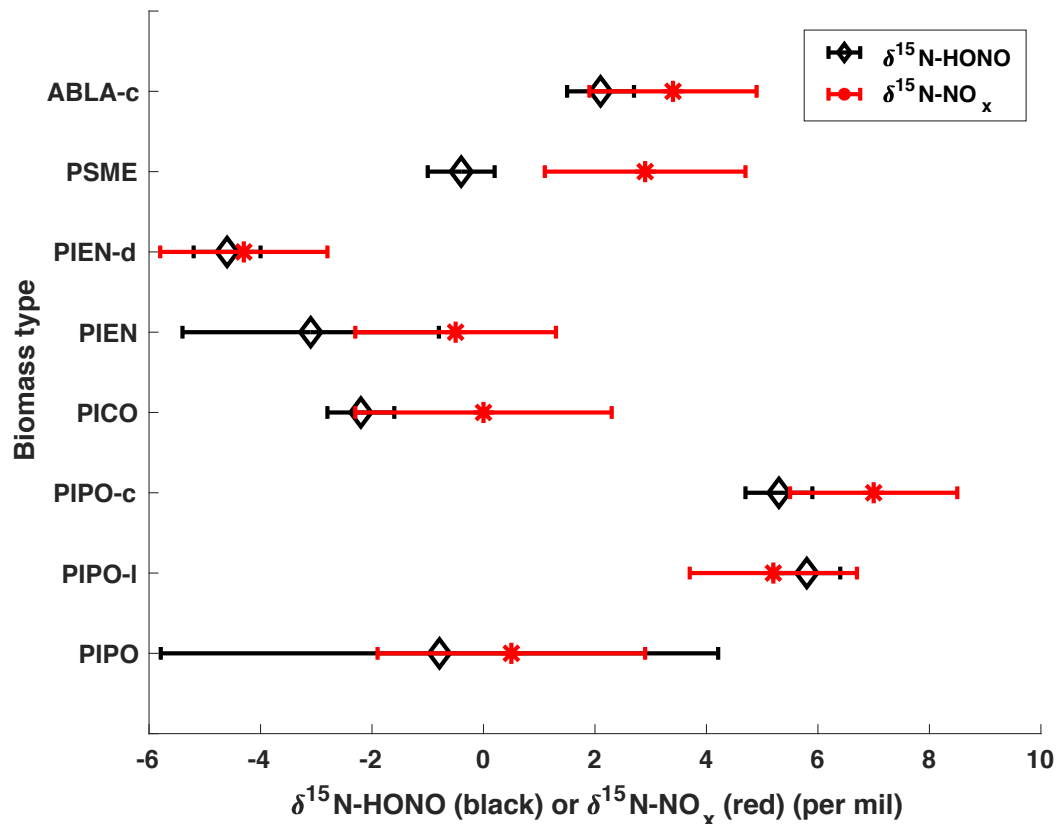
Figure 4. Concentration weighted mean $\delta^{15}N$- of HONO and NO_x versus biomass type. The error bars are propagation of replicate $\pm 1\sigma$ uncertainty (when n>1) and method uncertainty; otherwise, the error bars stand for method uncertainty. PIPO is ponderosa pine, PICO is lodgepole pine, PIEN is Engelmann spruce, PSME is Douglas-fir, ABLA is subalpine (from Fish Lake, canopy). l indicates litter, c indicates canopy, d indicates duff.

δ^{15}N-biomass = (0.42±0.17) δ^{15}N-NO$_x$ + 1.30

(R^2=0.71, p-value<0.001, 2σ)

1019
1020
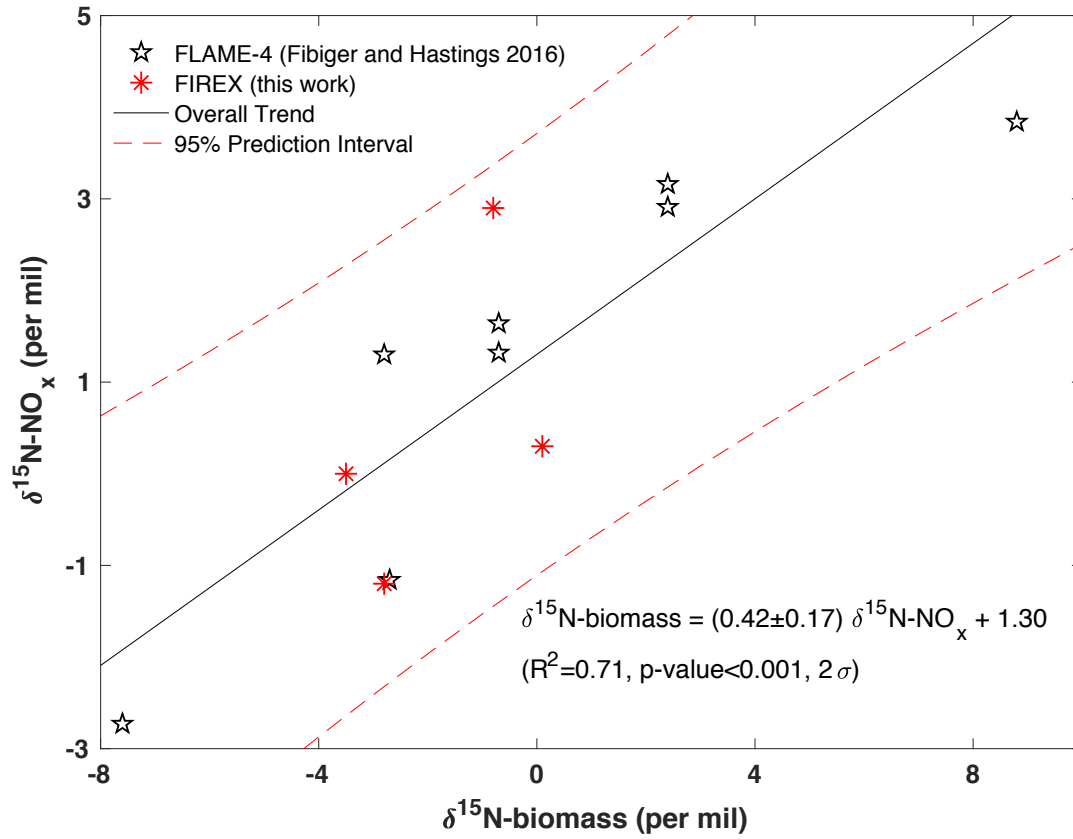1021 **Figure 5.** Dependence of δ^{15}N-NO$_x$ on δ^{15}N-biomass. Star data points represent results
1022 from FLAME-4 study (Fibiger and Hastings, 2016); Asterisk data points represent results
1023 from this work; solid line is linear regression between δ^{15}N-NO$_x$ and δ^{15}N-biomass for
1024 the combined dataset; dashed lines are 95% prediction interval (2σ).

1025
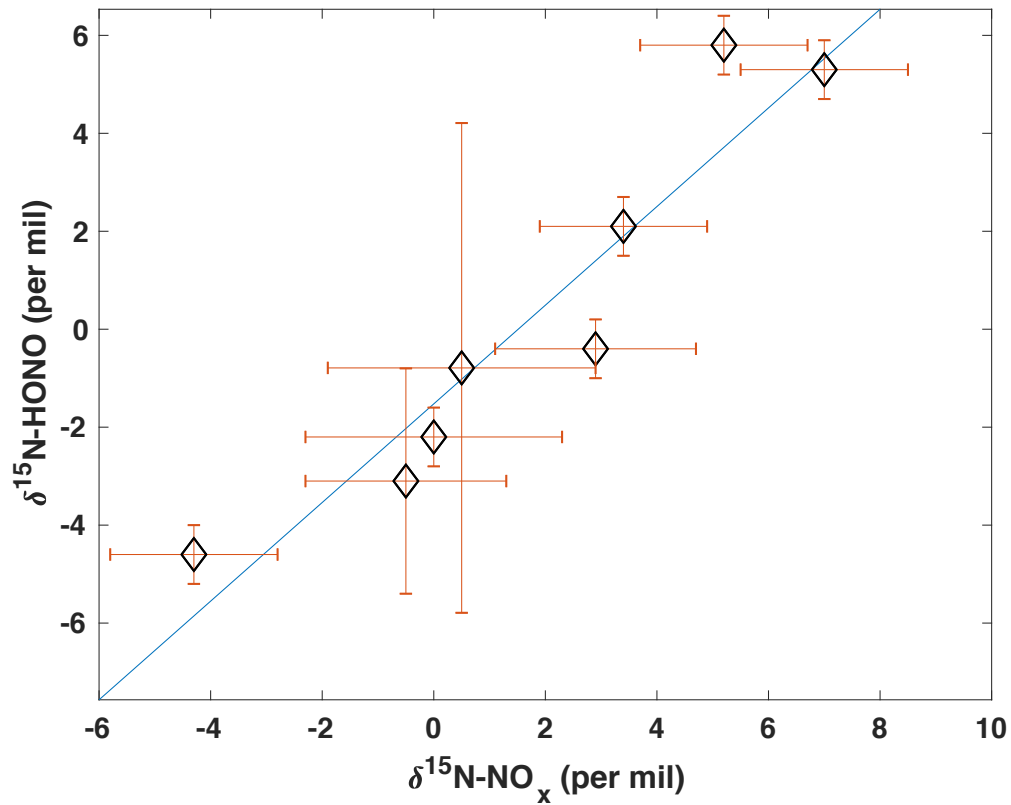**Figure 6.** Scatter plot between δ^{15}N-HONO and δ^{15}N-NO$_x$. All error bars are propagation
1026
of replicate uncertainty ($\pm 1\sigma$) and method uncertainty. Linear regression follows δ^{15}N-
1027
HONO = 1.01 δ^{15}N-NO$_x$ - 1.52 (R^2 = 0.89, p<0.001).
1028

1029
1030
1031
1032
1033
1034
1035
1036
1037
1038
1039
1040
1041
1042
1043
1044
1045
1046
1047
1048
1049

Isotopic characterization of nitrogen oxides (NO$_x$), nitrous acid (HONO), and nitrate (NO$_3^-$(p)) from laboratory biomass burning during FIREX

Jiajue Chai[1], David J. Miller[1,a], Eric Scheuer[2], Jack Dibb[2], Vanessa Selimovic[3], Robert Yokelson[3], Kyle J. Zarzana[4,5,b], Steven S. Brown[4,6], Abigail R. Koss[4,5,6,c], Carsten Warneke[5,6], Meredith Hastings[1]

1. Department of Earth, Environmental and Planetary Sciences, and Institute at Brown for Environment and Society, Brown University, Providence, RI, USA
2. Institute for the Study of Earth, Ocean and Space, University of New Hampshire, Durham, NH, USA
3. Department of Chemistry, University of Montana, Missoula, USA
4. Chemical Sciences Division, NOAA Earth System Research Laboratory, Boulder, CO, USA
5. Cooperative Institute for Research in Environmental Sciences, University of Colorado, Boulder, CO, USA
6. Department of Chemistry, University of Colorado, Boulder, CO, USA
a. Now at: Environmental Defense Fund, Boston, MA, USA
b. Now at: Department of Chemistry, University of Colorado, Boulder, CO, USA
c. Department of Civil and Environmental Engineering, Massachusetts Institute of Technology, Cambridge, MA, USA

Correspondence: Jiajue Chai (jiajue_chai@brown.edu)

Experimental details

NO$_x$ online concentration measurement

NO and NO$_x$ concentrations were measured with a Thermo Scientific Model 42i chemiluminescence NO/NO$_x$ analyzer, with ±0.4 ppbv precision and 0.2 ppbv zero noise at 1 minute time resolution. In the NO channel, O$_3$ generated by an ozonator titrates NO to excited state NO$_2$ which subsequently produces luminescence that is proportional to NO concentration. In the NO$_x$ channel, the sample gas stream first flows through a heated molybdenum catalyst (325 °C) that converts NO$_2$ to NO before entering the NO+O$_3$ reaction chamber. The auto cycle mode (NO/NO$_x$) switches the mode solenoid valve automatically on a 10 second cycle so that NO, NO$_2$, and NO$_x$ concentrations are determined. It is known that some NO$_y$ species including HONO, HNO$_3$, organic nitrate and PAN can be partially converted to NO in the hot molybdenum catalyst, causing positive artifacts in measured NO$_x$ (Reed et al., 2016). In this study, only the HONO interference was corrected for. This was done by subtracting the ADS measured HONO concentration (mean value across each whole fire) from Thermo analyzer measured NO$_x$

concentration averaged across the whole fire; this provided the approximate lower limit of the NO_x concentration by assuming HONO is 100% converted to NO on the Molybdenum catalyst (e.g. (Dunlea et al., 2007; Febo et al., 1995). Contributions from HNO_3, PAN and gaseous organic nitrate are not of major concern because no photo-oxidation is involved in indoor fires (Koss et al., 2018; Selimovic et al., 2018; Stockwell et al., 2014). In addition, we do not expect that other reactive nitrogen species such as NH_3 and hydrogen cyanide (HCN) interfere with NO_2 measurement. A particulate matter filter (Millipore, 1μm PTFE) was always placed before the inlet of the NO_x analyzer. The NO channel was calibrated before and after the entire Fire Lab experiments with standard NO (10 ppmv in N_2) diluted with zero air (Thermo Fisher Scientific, Model 111) via a gas dilution calibrator (Thermo Fisher Scientific, Model 146i) and NO_2 response of the NO_x channel using O_3 titration is within ±5% accuracy. The NO_x measurement verified the concentration of the NO_x collected for isotopic analysis, and the original NO_x data is available in the NOAA FIREX archive (FIREX, 2016).

Table S1 Information of fuels measured for $\delta^{15}N$-biomass. Acronyms: ponderosa pine (PIPO), lodgepole pine (PICO), Engelmann spruce (PIEN), Douglas-fir (PSME) and subalpine fir (ABLA). Each fuel is a mixture of one or multiple compositions (different parts from the vegetation) including duff, litter, canopy, rotten, shrub. $\delta^{15}N$ of each composition (5th column) was measured in replicates using the method described in section 2.2.3. Composition mass weighted $\delta^{15}N$ in 6th column are calculated by mass weighting $\delta^{15}N$ of each composition (5th column) with nitrogen content (=sample weight×%N). Mixture mass weighted $\delta^{15}N$ (8th column) is calculated by mass weighting $\delta^{15}N$ (6th column) with fraction in mixture (7th column).

Sample	Fuel Compo.	Sample Weight (mg)	%N	$\delta^{15}N$ (‰)	Compo. Mass Weighted $\delta^{15}N$ ‰	Fraction in Mixture	Mixture Mass Weighted $\delta^{15}N$ (‰)
PIPO	Duff	4.87	1.11	0.32	0.39	0.16	0.1
PIPO	Duff	5.00	1.11	0.31			
PIPO	Duff	5.36	1.20	0.51			
PIPO	Litter	4.75	0.57	1.27	0.94	0.29	
PIPO	Litter	7.60	0.54	0.59			
PIPO	Canopy	4.76	0.9	-0.11	-0.10	0.31	

			7				
PIPO	Canopy	5.16	0.97	-0.10			
PIPO	Rotten	7.06	0.19	1.15	-1.33	0.18	
PIPO	Rotten	10.14	0.17	-2.29			
PIPO	Rotten	10.30	0.16	-1.55			
PIPO	Rotten	10.37	0.18	-2.82			
PICO	Duff	4.69	0.51	-2.95	-2.53	0.20	-3.5
PICO	Duff	16.31	0.42	-1.83			
PICO	Duff	10.58	0.68	-2.63			
PICO	Litter	4.45	0.84	-2.73	-3.09	0.11	
PICO	Litter	4.75	0.91	-3.38			
PICO	Litter	7.06	0.85	-3.15			
PICO	Canopy	4.45	0.93	-4.17	-4.16	0.40	
PICO	Canopy	5.24	0.88	-4.14			
PICO	Shrub	4.48	0.90	-3.51	-3.36	0.09	
PICO	Shrub	6.60	0.88	-3.21			
PSME	Duff	4.90	0.74	-0.08	0.39	0.15	-0.8
PSME	Duff	9.95	0.87	0.79			
PSME	Litter	4.53	0.72	-2.41	-2.30	0.11	
PSME	Litter	6.69	0.72	-2.19			
PSME	Canopy	4.66	0.87	-2.59	-2.33	0.46	
PSME	Canopy	5.99	0.86	-2.08			
PSME	Rotten	7.76	0.31	2.02	1.67	0.28	
PSME	Rotten	7.08	0.3	1.74			

PSME	Rotten	10.09	10.30	1.23			
Chamise	Canopy	5.27	1.14	-3.03	-2.84		
Chamise	Canopy	5.42	1.14	-2.66			
PIEN	Duff	4.68	1.32	-1.38	-1.41	0.17	-2.8
PIEN	Duff	5.03	1.40	-1.43			
PIEN	Canopy	4.59	0.95	-3.95	-3.50	0.31	
PIEN	Canopy	6.19	0.95	-2.70			
PIEN	Canopy	5.48	0.98	-3.84			
ABLA	Duff	5.25	1.17	-1.57	-1.40		
ABLA	Duff	6.47	1.20	-1.25			
ABLA	Litter	4.38	1.00	-4.02	-3.85		
ABLA	Litter	6.24	0.91	-3.66			

Table S2 Comparisons between $[HONO]_{ADS}$ with mean values of various high resolution methods including MC/IC, FTIR, CES and PTR-ToF. Missing data points are results of instrumental issues.

Fire no.	ADS(ppb)	MCIC(ppb)	CES(ppb)	FTIR(ppb)	PTR-ToF (ppb)
8	25.7	25.7	22.4	29.5	29.5
9	21.3	24.9	19.7	--	--
10	42.2	44.2	46.6	--	--
11	112.3	69.8	103.3	--	--
14	25.3	24.5	35.6	25.7	41.3
15	51.0	76.2	58.9	37.9	50.2
16	70.0	56.4	70.1	56.4	--
17	47.1	53.3	39.4	35.1	--
18	45.3	38.3	50.0	41.3	50.0
19	23.8	41.5	28.4	24.3	30.9
20	52.5	42.9	56.8	41.9	--
21	9.9	6.0	--	7.0	16.2
22	40.0	32.0	--	14.5	42.1

Table S3 Data for NOx concentration measured by NOx analyzer and NOx collection system.

Fire #	$NO_x\_analyzer$ (ppb)	$NO_x\_collected$ (ppb)
2	113.5	147.9
3	151.3	124.7
5	182.7	123.8
6	60.2	94.7
7	313.0	398.3
8	100.5	91.7
9	80.5	73.6
10	156.2	229.7
11	498.9	571.8
12	33.9	36.2
14	39.5	70.0
15	38.9	43.5
16	338.3	443.3
19	84.3	73.3
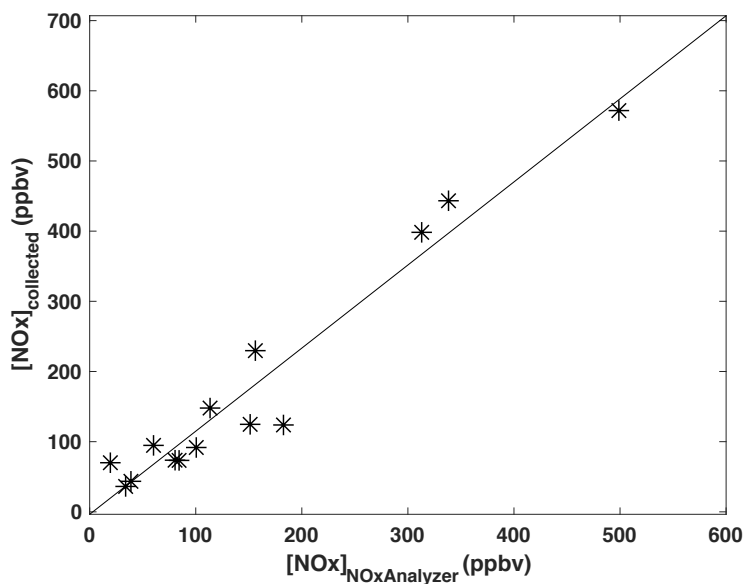
Figure S1 NO_x concentration comparison between NO_x analyzer measurement (mean value over the entire fire) and NO_x collected by the collection system for isotopic

analysis. Solid line is linear regression of the dataset: y = (1.18±0.08)x + (-3.5±17.2), with R^2 = 0.94, p_{slope} < 0.001, $p_{intercept}$=0.84, and uncertainty=1σ.
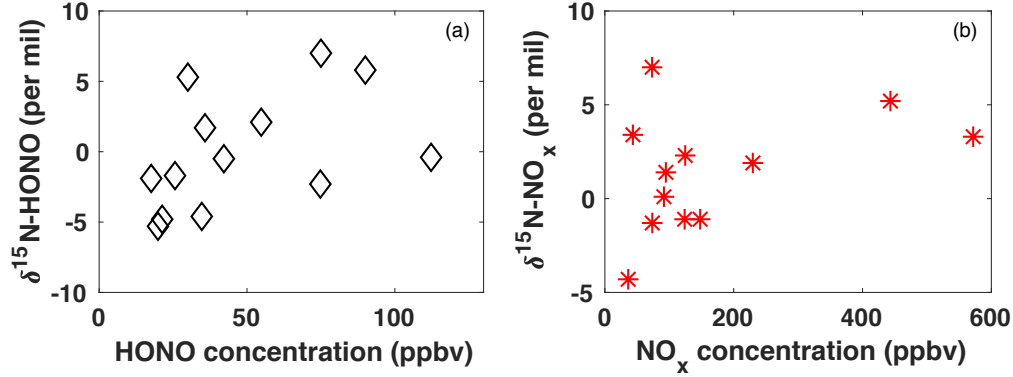

Figure S2. Relationship between $\delta^{15}N$ value versus concentration for HONO (a) and NO_x (b). p-values for linear correlation are 0.12 (a) and 0.93 (b) respectively.
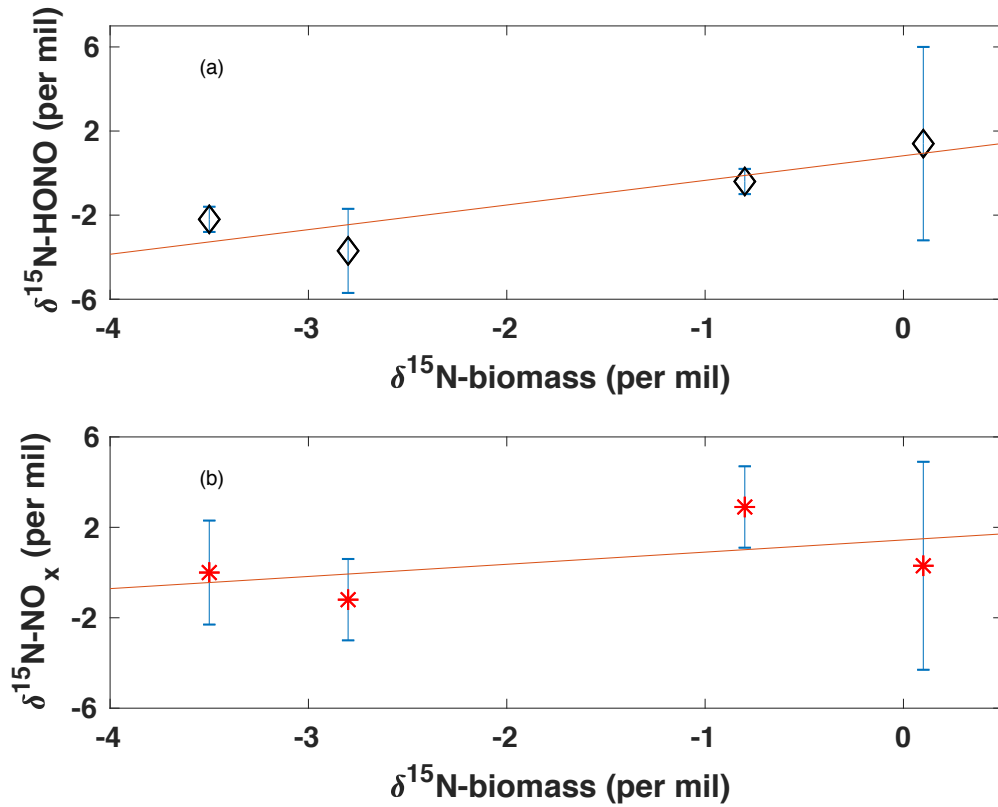

Figure S3. Linear regressions between **(a)** $\delta^{15}N$-HONO and $\delta^{15}N$-biomass, $\delta^{15}N$-HONO = 1.2 $\delta^{15}N$-biomass + 0.80 (r^2=0.83, p_{slope}=0.1), and **(b)** $\delta^{15}N$-NO_x and $\delta^{15}N$-biomass

δ^{15}N-NO$_x$ = 0.54δ^{15}N-biomass + 1.4 (r^2=0.28, p_{slope}=0.5).
The error bars are propagation of replicate uncertainty (1σ) and method uncertainty.

References

Dunlea, E. J., Herndon, S. C., Nelson, D. D., Volkamer, R. M., San Martini, F., Sheehy, P. M., Zahniser, M. S., Shorter, J. H., Wormhoudt, J. C., Lamb, B. K., Allwine, E. J., Gaffney, J. S., Marley, N. A., Grutter, M., Marquez, C., Blanco, S., Cardenas, B., Retama, A., Ramos Villegas, C. R., Kolb, C. E., Molina, L. T. and Molina, M. J.: Evaluation of nitrogen dioxide chemiluminescence monitors in a polluted urban environment, Atmospheric Chemistry and Physics, 7(10), 2691–2704, doi:https://doi.org/10.5194/acp-7-2691-2007, 2007.

Febo, Antonio., Perrino, Cinzia., Gherardi, Monica. and Sparapani, Roberto.: Evaluation of a High-Purity and High-Stability Continuous Generation System for Nitrous Acid, Environ. Sci. Technol., 29(9), 2390–2395, doi:10.1021/es00009a035, 1995.

FIREX: FIREX 2016 Fire Lab Data Archive, [online] Available from: https://esrl.noaa.gov/csd/groups/csd7/measurements/2016firex/FireLab/DataDownload/index.php?page=/csd/groups/csd7/measurements/2016firex/FireLab/DataDownload/ (Accessed 25 March 2019), 2016.

Koss, A. R., Sekimoto, K., Gilman, J. B., Selimovic, V., Coggon, M. M., Zarzana, K. J., Yuan, B., Lerner, B. M., Brown, S. S., Jimenez, J. L., Krechmer, J., Roberts, J. M., Warneke, C., Yokelson, R. J. and Gouw, J. de: Non-methane organic gas emissions from biomass burning: identification, quantification, and emission factors from PTR-

ToF during the FIREX 2016 laboratory experiment, Atmospheric Chemistry and Physics, 18(5), 3299–3319, doi:https://doi.org/10.5194/acp-18-3299-2018, 2018.

Reed, C., Evans, M. J., Carlo, P. D., Lee, J. D. and Carpenter, L. J.: Interferences in photolytic NO_2 measurements: explanation for an apparent missing oxidant?, Atmospheric Chemistry and Physics, 16(7), 4707–4724, doi:https://doi.org/10.5194/acp-16-4707-2016, 2016.

Selimovic, V., Yokelson, R. J., Warneke, C., Roberts, J. M., de Gouw, J., Reardon, J. and Griffith, D. W. T.: Aerosol optical properties and trace gas emissions by PAX and OP-FTIR for laboratory-simulated western US wildfires during FIREX, Atmos. Chem. Phys., 18(4), 2929–2948, doi:10.5194/acp-18-2929-2018, 2018.

Stockwell, C. E., Yokelson, R. J., Kreidenweis, S. M., Robinson, A. L., DeMott, P. J., Sullivan, R. C., Reardon, J., Ryan, K. C., Griffith, D. W. T. and Stevens, L.: Trace gas emissions from combustion of peat, crop residue, domestic biofuels, grasses, and other fuels: configuration and Fourier transform infrared (FTIR) component of the fourth Fire Lab at Missoula Experiment (FLAME-4), Atmos. Chem. Phys., 14(18), 9727–9754, doi:10.5194/acp-14-9727-2014, 2014.